Updated Excitation and Ionization Cross Sections for Electron Impact on Atomic Oxygen

Russ R. Laher and Forrest R. Gilmore

R&D Associates, Marina del Rey, California 90295

Cross sections for the excitation and ionization of atomic oxygen by electron impact are presented as the result of a critical review of experimental and theoretical work on this subject. An effort has been made to compile the most accurate and complete set of cross sections available. More than 60 profiles of excitation cross section versus electron-impact energy are presented. These include transitions to the forbidden metastable $O(2p^4\,{}^1D)$ and $O(2p^4\,{}^1S)$ states, the allowed autoionizing $O(2p^5\,{}^3P^o)$ state, nine allowed Rydberg series, and twenty-nine forbidden Rydberg series. Recommended ionization cross sections for transitions to the outer-electron ionization states $O^+({}^4S^o)$, $O^+({}^2D^o)$, $O^+({}^2P^o)$, to the inner-electron ionization state $O^+({}^4P)$, and to the O^{2+} state are also given. Many of these excitation and ionization cross sections are based on recently published laboratory measurements, and differ from previously accepted values by factors of ~ 2–3, and in a few cases by up to a factor of 10. The data presented in this report will be useful in calculations of aeronomical and artificially-induced electron impact on atomic oxygen, an important component of the upper atmosphere.

Key words: atomic oxygen; critical review; cross-section data; electron energy deposition; electron impact; excitation; ionization.

Contents

1. Introduction

Electron-impact cross sections of atmospheric gases are needed as input data for calculations of the chemical and radiative properties of the atmosphere when bombarded by

electrons from various natural and artificial sources. These sources include auroral electrons from the sun, fast electrons (beta rays) from the fission products of nuclear bursts, and photoelectrons produced by the ultraviolet and x rays from the sun or from nuclear bursts.

At altitudes above ~90 km atomic oxygen is a major atmospheric constituent. Until recently the available measurements of the cross sections for exciting this gas to its various electronic and ionic states were quite limited, due to the experimental difficulties in working with this very reactive species. However, over the last three years there has been renewed activity in this subject, and several pertinent experimental papers have been published. This new information has prompted the present review and compilation, which combines the new data with the older measurements and theoretical results to derive a reasonably complete and accurate set of cross sections, although some cross sections are still uncertain by a factor of 2 or so.

Before discussing in sequence the cross sections for ex-

citing specific electronic states, it is useful to note some general characteristics of the theoretical calculations and measurements. Existing theoretical calculations generally have uncertainties of a factor of 2 or greater, except at electron energies above ~200 eV. However, theory is very useful for extrapolating measurements to high energies, and for obtaining approximate cross sections where accurate measurements have not been made.

Measurements of the total ionization cross section of a gas by electrical means are relatively simple and direct. However, measurements of the cross section for exciting a given electronic state of an atom or ion are more difficult. In atomic oxygen, two methods have been used. In the optical method, radiation from the excited state is detected and measured. The biggest problem with this method is that the bombarding electrons generally excite many higher states, some of which may radiatively cascade down to the state of interest, giving an apparent cross section which is larger than the true direct cross section. In some cases the cascade con-

Table 1. Excited and ionized states of atomic oxygen included in this report.

Final state	Threshold (eV)	Final state	Threshold (eV)
$O(^1D)$	1.96	$O(4d'\ ^1SPDFG^\circ)$	16.07
$O(^1S)$	4.18	$O(ns'\ ^3D^\circ)$	16.46*
		$O(ns'\ ^1D^\circ)$	16.47*
$O(2p^5\ ^3P^\circ)$	15.65	$O(np'\ ^3PDF)$	16.54*
		$O(np'\ ^1PDF)$	16.54*
$O(3s\ ^5S^\circ)$	9.14	$O(nd'\ ^3SPD^\circ)$	16.65*
$O(3s\ ^3S^\circ)$	9.51	$O(nd'\ ^3FG^\circ)$	16.65*
$O(3p\ ^5P)$	10.73	$O(nd'\ ^1SPDFG^\circ)$	16.66*
$O(3p\ ^3P)$	10.98		
$O(3d\ ^5D^\circ)$	12.07	$O(3s''\ ^3P^\circ)$	14.11
$O(3d\ ^3D^\circ)$	12.08	$O(3s''\ ^1P^\circ)$	14.36
$O(4s\ ^5S^\circ)$	11.83	$O(3p''\ ^3SPD)$	15.77
$O(4s\ ^3S^\circ)$	11.92	$O(3p''\ ^1SPD)$	15.99
$O(4p\ ^5P)$	12.28	$O(3d''\ ^3P^\circ, ^3D^\circ)$	17.09
$O(4p\ ^3P)$	12.35	$O(3d''\ ^3F^\circ)$	17.09
$O(4d\ ^5D^\circ)$	12.74	$O(3d''\ ^1PDF^\circ)$	17.09
$O(4d\ ^3D^\circ)$	12.75	$O(4s''\ ^3P^\circ)$	16.81
$O(ns\ ^5S^\circ)$	13.13*	$O(4s''\ ^1P^\circ)$	16.90
$O(ns\ ^3S^\circ)$	13.15*	$O(4p''\ ^3SPD)$	17.24
$O(np\ ^5P)$	13.22*	$O(4p''\ ^1SPD)$	17.25
$O(np\ ^3P)$	13.24*	$O(4d''\ ^3PD^\circ)$	17.77
$O(nd\ ^5D^\circ)$	13.33*	$O(4d''\ ^3F^\circ)$	17.77
$O(nd\ ^3D^\circ)$	13.33*	$O(4d''\ ^1PDF^\circ)$	17.77
		$O(ns''\ ^3P^\circ)$	18.15*
$O(3s'\ ^3D^\circ)$	12.53	$O(ns''\ ^1P^\circ)$	18.16*
$O(3s'\ ^1D^\circ)$	12.72	$O(np''\ ^3SPD)$	18.22*
$O(3p'\ ^3PDF)$	14.06	$O(np''\ ^1SPD)$	18.22*
$O(3p'\ ^1PDF)$	14.20	$O(nd''\ ^3PD^\circ)$	18.35*
$O(3d'\ ^3S^\circ, ^3P^\circ, ^3D^\circ)$	15.36	$O(nd''\ ^3F^\circ)$	18.35*
$O(3d'\ ^3FG^\circ)$	15.39	$O(nd''\ ^1PDF^\circ)$	18.35*
$O(3d'\ ^1SPDFG^\circ)$	15.40		
$O(4s'\ ^3D^\circ)$	15.17	$O^+(^4S^\circ)$	13.61
$O(4s'\ ^1D^\circ)$	15.22	$O^+(^2D^\circ)$	16.93
$O(4p'\ ^3PDF)$	15.59	$O^+(^2P^\circ)$	18.63
$O(4p'\ ^1PDF)$	15.58	$O^+(^4P)$	28.49
$O(4d'\ ^3SPD^\circ)$	16.08		
$O(4d'\ ^3FG^\circ)$	16.07	O^{2+}	48.77

* Average energy of $n = 5$ and ∞ (ionization limit) states

tribution is known to be small; in others it can be determined by measuring the intensity of the cascade radiation, although this may lie in an inconvenient spectral region. Other important limitations of this method are that it cannot measure cross sections for exciting metastable (nonradiating) states, and, for high-lying radiating states that also autoionize, it measures only the fraction that does not autoionize. In addition, until recently absolute calibrations of optical measurements in some spectral regions have had uncertainties of a factor of 2 or more.

A more direct method of measuring an excitation cross section is to measure the fraction of the incident electrons that have lost an amount of energy equal to the excitation energy of the state under consideration. This method, however, is experimentally more difficult, and only with improved techniques in the last few years has it given accurate results.

Table 1 gives the final states of atomic oxygen transitions considered in this report, along with the corresponding threshold energies (Moore, 1976). These final states and threshold energies are also shown in the energy level diagrams given in Figs. 1 and 2. The threshold energies for Ryd-
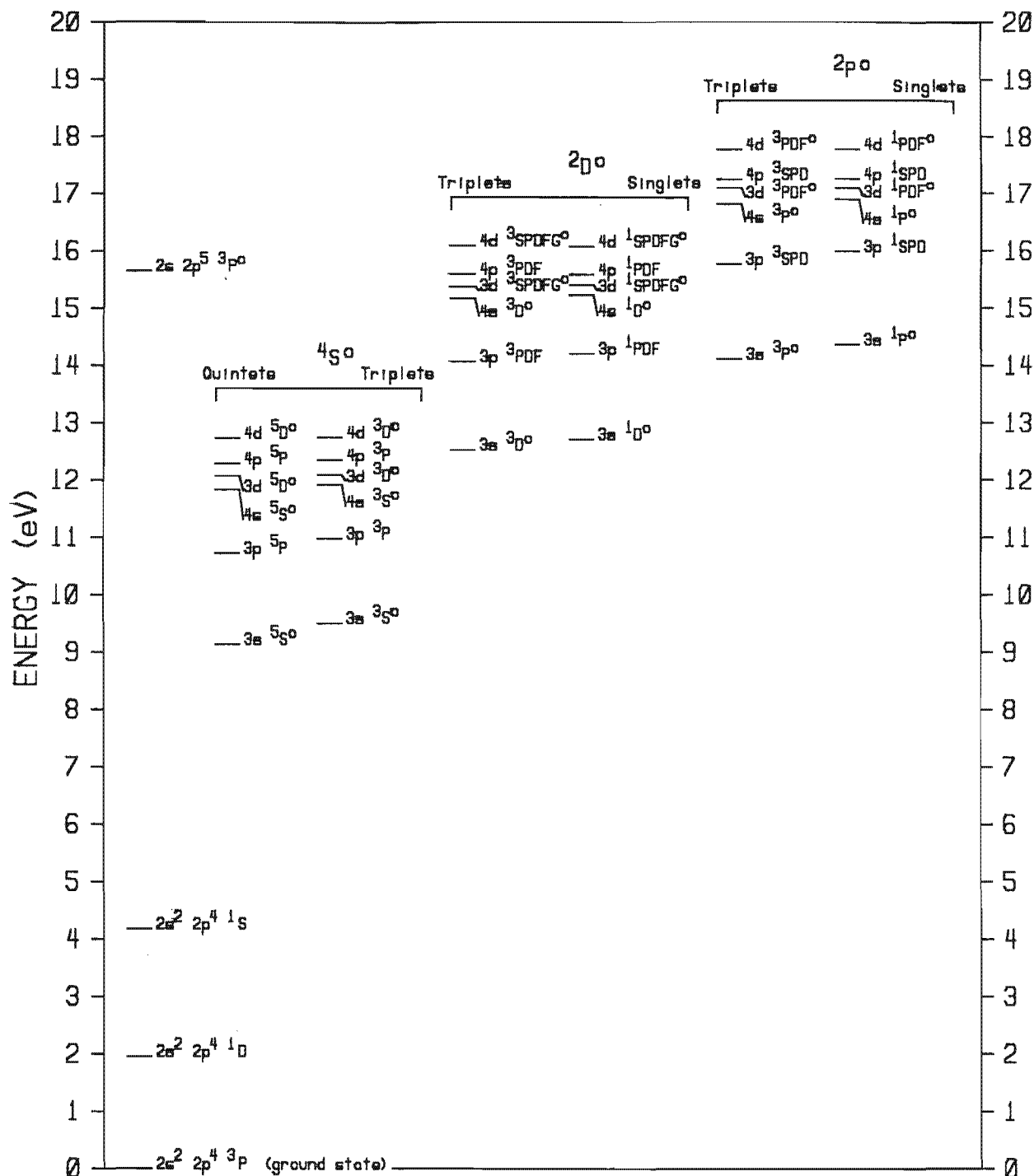
FIG. 1. Atomic oxygen threshold energies for electronic excitation to lower excited states.
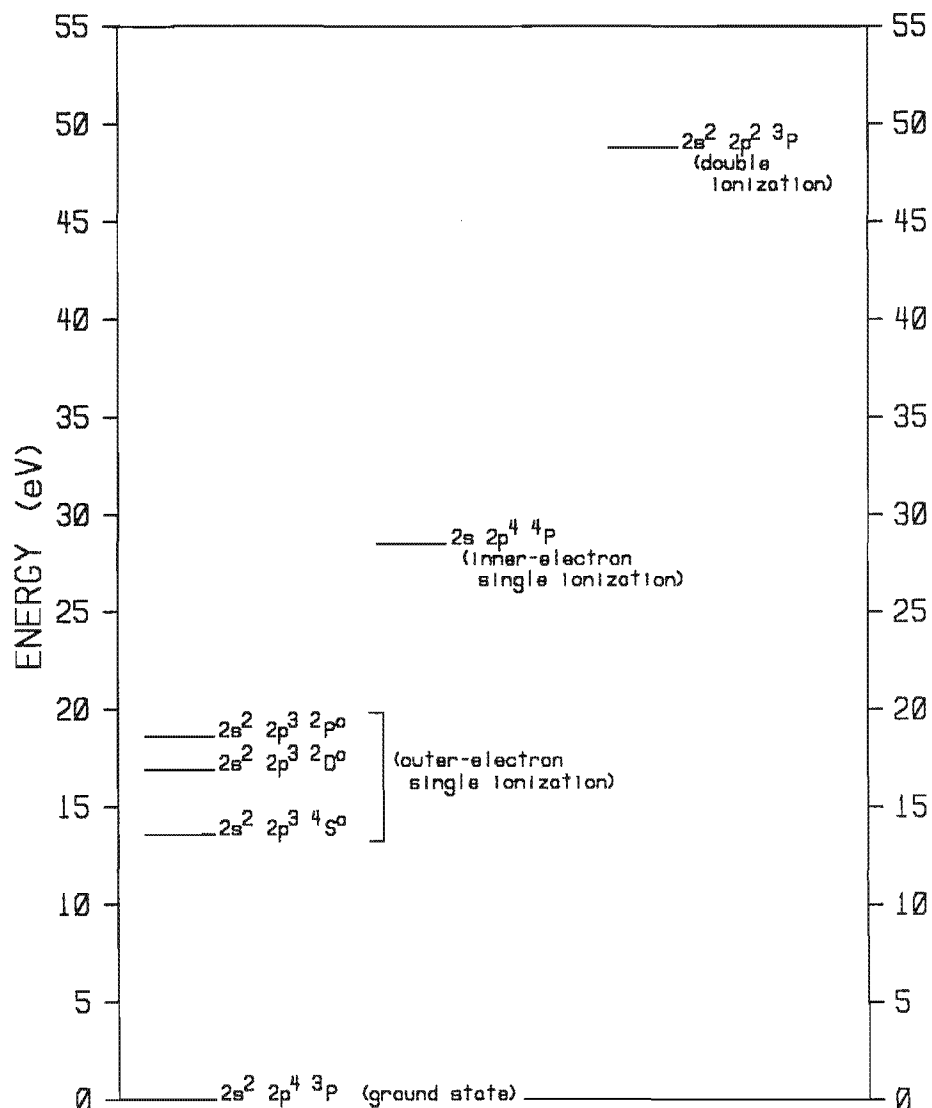
FIG. 2. Atomic oxygen threshold energies for ionization to single and double ion states.

berg excitations, where not available from measurements, are computed using the well-known formula

$$W_n = W_I - \frac{R}{(n - \delta)^2},\qquad(1)$$

where the subscript n denotes nth state in the series, W_I is the ionization energy (series limit), R is the Rydberg energy, and δ is the quantum defect for the series. Values of W_I are listed in Table 1, and values of δ for the Rydberg series considered in this report, obtained from Jackman et al. (1977), are given in Table 2. In all cases the initial state prior to the inelastic electron scattering is the $2s^2 2p^4 \; ^3P$ ground state of atomic oxygen. Only transitions to states with angular momentum orbitals $s, s', s'', p, p', p'', d, d'$, and d'' (where the unprimed, primed, and double-primed orbital symbols refer to the $^4S^o$, $^2D^o$, and $^2P^o$ ion cores of the excited states of atomic oxygen, respectively) are considered. Electron-impact cross sections for higher angular momentum states are not available, but theoretical considerations indicate that they are generally small. For certain sets of high states with

similar electron configurations and energy thresholds, such as the $O(4d'\; ^3F^o)$ and $O(4d'\; ^3G^o)$ states, we present only the sum of the cross sections, and use the notation $O(4d'\; ^3 FG^o)$ to refer to this sum. The cross sections as a function of electron-impact energy are presented in both graphical and tabular form, with inclusion of formulas in the tables for extrapolating these values to higher energies.

In an earlier report Slinker and Ali (1986), in connection with a calculation of excitation and electron energy loss in bombarded atomic oxygen, tabulated a number of electron-impact cross sections for this species. However, this tabulation was based on older data, much of which has since been superseded. For allowed transitions many of the new values differ by factors of ~2–3 from the older cross sections. For low-lying metastable excitations the new measurements show that the cross section falls off more gradually with increasing energy in the 10–30 eV range than the E^{-3} fall off assumed by Slinker and Ali. New cross sections for higher forbidden transitions that are now available, from both energy-loss and optical measurements, allow better de-

Table 2. Quantum defects for Rydberg excitations.
Adapted from Jackman et al. (1977).

Rydberg state	δ
$ns\ {}^5S^o$	1.24
$ns\ {}^3S^o$	1.16
$np\ {}^5P$	0.81
$np\ {}^3P$	0.69
$nd\ {}^5D^o$	0.01
$nd\ {}^3D^o$	0.01
$ns'\ {}^3D^o$	1.21
$ns'\ {}^1D^o$	1.18
$np'\ {}^3P, {}^3D, {}^3F$	0.84
$np'\ {}^1P, {}^1D, {}^1F$	0.83
$nd'\ {}^3S^o, {}^3P^o, {}^3D^o, {}^3F^o, {}^3G^o$	0.04
$nd'\ {}^1S^o, {}^1P^o, {}^1D^o, {}^1F^o, {}^1G^o$	0.04
$ns''\ {}^3P^o$	1.25
$ns''\ {}^1P^o$	1.19
$np''\ {}^3S, {}^3P, {}^3D$	0.86
$np''\ {}^1S, {}^1P, {}^1D$	0.85
$nd''\ {}^3P^o, {}^3D^o, {}^3F^o$	0.05
$nd''\ {}^1P^o, {}^1D^o, {}^1F^o$	0.05

termination of cascade contributions, leading to cross sections that differ from the older values by up to a factor of 10. In addition, the earlier tabulation did not include some cross sections now known to be significant, such as the $2p^5\ {}^3P^o$ excitation. Finally, no information was given on autoionization, which has a cross section that is $\sim 20\%$ of the total inelastic cross section, and has a significant effect on the relative production of different O^+ states and on the energy distribution of the secondary electrons created in the ionization process. Application of the updated cross sections presented in this report to electron/oxygen-atom scattering calculations will provide more accurate values for excitation and ionization efficiencies, the secondary electron distribution, and the average electron energy lost per ion pair created.

2. Electron-Impact Excitation Cross Sections

2.1. Transitions to Non-Rydberg States

2.1.a. $O({}^3P \rightarrow 2p^4\ {}^1D)$

Shyn and Sharp (1986) have made measurements of the excitation cross section of the $O({}^3P \rightarrow 2p^4\ {}^1D)$ transition by electron impact at 7, 10, 15, 20, and 30 eV, using the electron energy-loss technique. These values, with an assigned 50% uncertainty, are within 20% of the theoretical results of Henry et al. (1969) and Vo Ky Lan et al. (1972). The theoretical results of Thomas and Nesbet (1975), which are available for electron-impact energies up to 10 eV, are also within 20% of the measurements at 7 and 10 eV. We fit the experimental data to a generalization of the semi-empirical formula of Jackman et al. (1977):

$$\sigma(E) = \frac{qF}{W^2(1 + \gamma E^2/W^2)} \left[1 - \left(\frac{W}{E}\right)^\alpha \right]^\beta \left(\frac{W}{E}\right)^\Omega ,$$

$$(2)$$

where $\sigma(E)$ is the cross section in units of cm^2, E is the electron-impact energy in units of eV, $q = 4\pi a_o^2 R^2 = 6.513 \times 10^{-14}$ cm^2 eV^2 (a_o is the Bohr radius and R is the Rydberg energy), W is the threshold energy of the excitation in eV, and F, α, β, Ω, and γ are adjustable parameters for use in fitting the formula to the experimental data. We have added the γ term to the Jackman et al. formula so that (with $\Omega = 1$) the cross section for this transition has an E^{-3} asymptotic behavior at high energies ($E > 200$ eV) as required for spin-forbidden transitions (Henry et al., 1969). Using $W = 1.96$ eV, and the parameters $F = 0.012$, $\alpha = 1$, $\beta = 2$, and $\Omega = 1$ from Jackman et al. (1977), and $\gamma = 0.002$, Eq. (2) yields values for the $O({}^3P \rightarrow 2p^4\ {}^1D)$ cross section that agree well with the theoretical results for energies lower than 7 eV, and fit the measurements of Shyn and Sharp (1986) within 30%. The cross sections computed using Eq. (2) are shown in Fig. 3, and are tabulated in Table 3.

2.1.b. $O({}^3P \rightarrow 2p^4\ {}^1S)$

Shyn et al. (1986) have measured the cross section of the $O({}^3P \rightarrow 2p^4\ {}^1S)$ excitation at 10, 15, 20, and 30 eV. In these measurements the direct method of electron energy-loss was used. While the experimental profile shape in the 10–30 eV range closely resembles the theoretical cross-section curves of Henry et al. (1969) and Vo Ky Lan et al. (1972), the experimental data are greater in magnitude by a factor of 2. Note, however, that the data have a 54% uncertainty. To fit the excitation cross sections for this transition as a function of electron-impact energy, we use Eq. (2) with $W = 4.18$ eV, $F = 0.006$, $\alpha = 0.5$, $\beta = 1$, $\Omega = 1$, and $\gamma = 0.0004$, where the values of α, β, and Ω are from Jackman et al. (1977). Given the large error bars on the experimental data and the large differences between the experimental and theoretical cross sections, we have chosen the parameter F such that $\sigma(E)$ peaks at a value intermediate to the recent measurement and the theoretical result at 10 eV. Figure 3 and Table 3 present the recommended cross sections for this transition.

2.1.c. $O({}^3P \rightarrow 2p^5\ {}^3P^o)$

The only experimental cross sections for the excitation of $O(2p^5\ {}^3P^o)$ are those of Vaughan and Doering (1988), obtained from electron energy-loss measurements. The curve shown in Fig. 3 is based on the experimental data at 30, 50, 100, 150, and 200 eV. We have reduced the measurement at 150 eV by 16% to smooth the cross section, given the large error bar on this particular datum.

For energies greater than ~ 200 eV, the excitation cross section for an allowed transition can be approximated by the formula

$$\sigma(E) = \frac{A + (qF/W) \ln E}{E} ,$$

$$(3)$$

where A is a constant, q and W have been defined in Sec. 2.1.a., and F is the optical oscillator strength (Jackman et al., 1977). For this transition, $F = 0.070$ (Doering et al.,

FIG. 3. O($^3P \rightarrow 2p^4\ ^1D$, $2p^4\ ^1S$, $2p^5\ ^3P^o$) excitation cross sections.

Table 3. O($^3P \longrightarrow 2p^4\ ^1D$, $2p^4\ ^1S$, $2p^5\ ^3P^o$) excitation cross sections.

Electron energy (eV)	$\sigma\ (10^{-18}\ cm^2)$		
	$2p^4\ ^1D$	$2p^4\ ^1S$	$2p^5\ ^3P^o$
2.1	0.82	-	-
2.4	5.41	-	-
2.7	10.7	-	-
3	15.4	-	-
4	24.9	-	-
4.4	26.7	0.54	-
4.8	27.7	1.30	-
5	28.0	1.60	-
6	28.3	2.57	-
7	27.4	3.02	-
8	26.0	3.22	-
9	24.4	3.28	-
10	22.8	3.27	-
12	19.8	3.15	-
14	17.1	2.97	-
16	14.8	2.79	0.17
18	12.9	2.61	1.27
20	11.2	2.44	2.09
25	8.07	2.09	4.11
30	5.90	1.80	6.82
40	3.34	1.37	12.7
45	2.58	1.21	13.6
50	2.02	1.07	14.1
55	1.61	0.95	13.7
70	0.87	0.69	11.5
100	0.33	0.38	7.45
150	0.11	0.16	4.49
200	0.05	0.08	3.14
>200	$4.0 \times 10^5 E^{-3}$	$6.4 \times 10^5 E^{-3}$	$(-914 + 291\ \ln E)/E$

1985), and we choose $A = -9.14 \times 10^{-16}$ cm^2 eV to give a smooth transition to the experimental data at lower energies. The cross sections are tabulated in Table 3.

2.2. Scaling of Cross Sections for Rydberg States

No cross section measurements are available for many of the Rydberg states of atomic oxygen. For these cross sections we have used a procedure of scaling from the measured cross sections of related Rydberg states, which is a generalization of the method of Jackman *et al.* (1977). These writers used semi-empirical cross section formulas, and assumed that the shape-controlling parameters in the formulas are the same for all the states in a given Rydberg series. This is nearly equivalent to assuming that all of the cross sections have the same shape, but scaled by a factor. For optically allowed transitions this factor is F/W, where F is the optical oscillator strength and W is the threshold energy for a given state in the series [see Eq. (3)]. For forbidden transitions, Eq. (2) with $\gamma = 0$ holds, and the F/W scaling holds (except near threshold) when $\Omega = 1$. For simplicity, the F/W scaling was also used for other values of Ω, since the relatively small variation in W among the states in a given Rydberg series makes this a reasonable approximation.

The known cross section for a Rydberg state of quantum number n can be used to calculate that of another state n' by using the relation

$$\sigma_{n'}(E) = \frac{W_n F_{n'}}{W_{n'} F_n}\sigma_n(E). \tag{4}$$

(This relation is not accurate very near the energy threshold,

where the curve must be shifted slightly to give the proper threshold behavior.) In this equaiton the F_n values are given by

$$F_n = \frac{F^*}{(n - \delta)^3}, \tag{5}$$

where F^* is a constant for a given Rydberg series which can be calculated using the quantum defect (Table 2) and a known optical oscillator strength for allowed transitions, or the known $\sigma_n(E)$ and Eq. (2) for forbidden transitions.

The cross sections for the higher Rydberg states, $n \geqslant 5$, are conveniently summed by approximating the different thresholds W_n by a single, intermediate value $W_A = (W_5 + W_I)/2$, and the sum by an integral (accurate to within a few percent):

$$\sigma_{n \geqslant 5}(E) \equiv \sum_{n=5}^{\infty} \sigma_n(E) = \sum_{n=5}^{\infty} \frac{W_3}{W_n}\frac{(3 - \delta)^3}{(n - \delta)^3}\sigma_3(E)$$

$$\approx \frac{W_3}{2W_A}\frac{(3 - \delta)^3}{(4.5 - \delta)^2}\sigma_3(E). \tag{6}$$

In writing Eq. (6) we have assumed that the $n = 3$ cross

section is the only cross section available in a given Rydberg series. For some of the Rydberg series treated in Secs. 2.3, 2.4, and 2.5, however, the $n = 4$ cross section or optical oscillator strength is available. In these cases the $\Sigma n \geqslant 5$ cross section is scaled from the $n = 4$ cross section, rather than the $n = 3$ cross section as done in Eq. (6).

2.3. Transitions to Rydberg States with an

$O^+(2s^2 2p^3 \, ^4S^o)$ Core

2.3.a. $O(^3P \to 3s \, ^5S^o)$

The only published measurements of these excitation cross sections are the optical data of Stone and Zipf (1974) which cover the electron-impact energy range of 11 to 70 eV. Above 25 eV, their data scatter by a factor of 2 or more about the mean. Later Zipf and Erdman (1985) determined that these measurements should be divided by a constant at least equal to 1.34, and possibly as large as 2.8, due to a re-evaluation of their measurement technique and a better measurement of their absolute calibration standard. If these data are divided by 2 they agree quite well with the theoretical calculations of Julienne and Davis (1976) for the excitation cross setion, including cascade contribution. These calculations indicate that over half of the optical cross section is due to cascade contributions, so that the Stone and Zipf measurements cannot be used alone to determine this excitation cross section. Evidence for the accuracy of the Julienne and Davis calculations is provided by their value for exciting the $3p \, ^5P$ state at 15 eV, which agrees well with the measurement (see Sec. 2.3.c.). Accordingly, we conclude that these theoretical results give the best values currently available for the excitation cross section of $O(^3P \to 3s \, ^5 \, S^o)$.
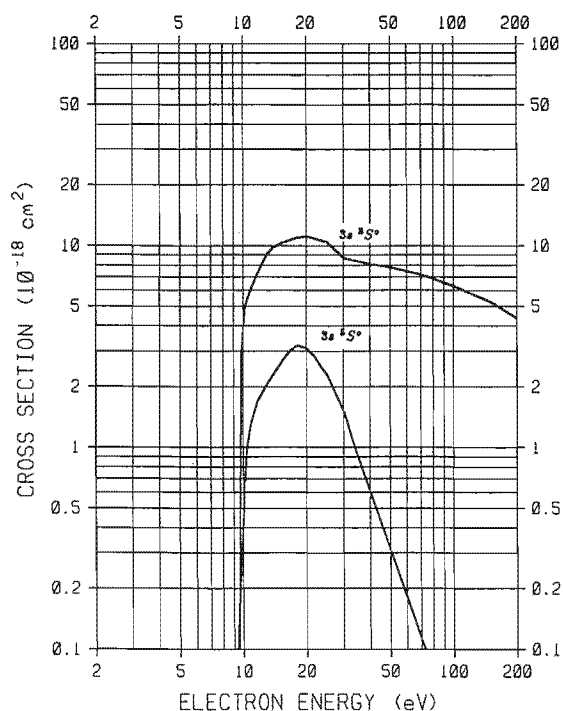
The recommended values are given in Fig. 4 and Table 4. For electron-impact energies $E > 50$ eV, the approximation

$$\sigma(E) = (3.88 \times 10^{-14} \, \text{cm}^2 \, \text{eV}^3) E^{-3} \tag{7}$$

is used. Equation (7) is consistent with the well-known high-energy behavior of spin-forbidden transitions.

2.3.b. $O(^3P \to 3s \, ^3 \, S^o)$

The $O(^3P \to 3s \, ^3S^o)$ excitation by electron impact is by far the most widely investigated of all atomic oxygen transitions. The latest measurements have been performed by Gulcicek and Doering (1988) and Vaughan and Doering (1986, 1987), who made electron energy-loss measurements in the 13.87–200 eV range. Previously Stone and Zipf (1971, 1974) employed optical measurement techniques and obtained larger values due to systematic errors and cascade contributions from higher states; however, the measurements were later lowered by 64% (Zipf and Erdman, 1985). According to Vaughan and Doering the revised optical cross sections of Zipf and Erdman, less reasonable cascade contributions, will yield values similar to theirs for impact energies greater than 30 eV; below 30 eV the agreement is not as good, the new measurements being roughly a factor of 1.2 larger than the optical data after cascade corrections are applied. The theoretical cross sections of Julienne and Davis (1976) and

FIG. 4. $O(^3P \to 3s \, ^5 \, S^o, 3s \, ^3S^o)$ excitation cross sections.

Table 4. $O(^3P \longrightarrow 3s \, ^5S^o, 3s \, ^3S^o)$ excitation cross sections.

Electron energy (eV)	$\sigma \, (10^{-18} \, \text{cm}^2)$	
	$3s \, ^5S^o$	$3s \, ^3S^o$
9.9	0.35	3.42
10.1	0.54	4.41
10.5	1.06	5.48
11	1.37	6.28
12	1.78	7.71
14	2.33	9.87
16	2.85	10.5
18	3.19	11.0
20	3.08	11.1
22	2.78	10.8
25	2.29	10.4
28	1.77	9.30
30	1.51	8.69
35	0.91	8.37
40	0.61	8.10
45	0.43	7.95
50	0.31	7.81
55	0.23	7.62
60	0.18	7.45
70	0.11	7.16
100	0.04	6.30
150	0.011	5.27
200	0.005	4.37
>200	$3.88 \times 10^4 E^{-3}$	$(-869 + 329 \ln E)/E$
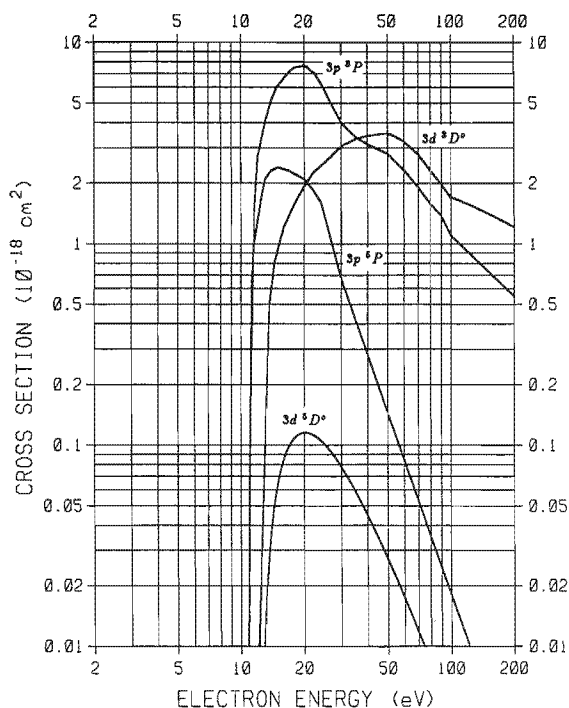
FIG. 5. $O(^3P \to 3p\,^5P, 3p\,^3P, 3d\,^5D^o, 3d\,^3D^o)$ excitation cross sections.

Rountree and Henry (1972) scaled upward by factors of 1.6 and 1.3, respectively, closely match the recent measurements. The theoretical results of Sawada and Ganas (1973) and Smith (1976) differ in variation with energy as well as magnitude from the recent measurements.

Thus the measurements of Gulcicek and Doering (1988) and Vaughan and Doering (1986, 1987) are in line with previous work. Assuming that technological advances over the years have produced a better laboratory apparatus, the newest measurements are preferred. The curve shown in Fig. 4 is a hand fit of the data; corresponding values are listed in Table 4. For impact energies > 200 eV, the cross sections are obtained from Eq. (3), where $F = 0.048$ (Doering et al., 1985) and $A = -8.69 \times 10^{-16}$ cm^2 eV.

2.3.c. $O(^3P \to 3p\,^5P, 3p\,^3P)$

Gulcicek et al. (1988) and Gulcicek and Doering (1987) report for the first time direct measurements of the excitation cross section for the $O(^3P \to 3p\,^5P)$ transition in the 13.87–30 eV range. Their results are fairly close to the calculated values of Julienne and Davis (1976). The semi-empirical cross section of Dalgarno and Lejeune (1971), which has a peak value of 1.7×10^{-18} cm^2 at 15 eV, is ~25% smaller than the experimental value.

We have used the direct measurements as a basis for

Table 5. $O(^3P \longrightarrow 3p\,^5P, 3p\,^3P, 3d\,^5D^o, 3d\,^3D^o)$ excitation cross sections.

Electron energy (eV)	σ $(10^{-18}$ cm$^2)$			
	$3p\,^5P$	$3p\,^3P$	$3d\,^5D^o$	$3d\,^3D^o$
11.1	0.22	0.15	-	-
11.3	0.71	0.47	-	-
11.5	1.00	1.42	-	-
12	1.31	2.72	-	-
14	2.31	5.22	0.041	0.62
16	2.35	6.63	0.087	1.22
18	2.23	7.52	0.109	1.59
20	2.10	7.70	0.116	1.94
22	1.86	7.13	0.113	2.26
24	1.61	6.26	0.105	2.45
26	1.18	5.32	0.096	2.64
28	0.88	4.58	0.087	2.85
30	0.67	4.00	0.078	3.06
35	0.42	3.41	0.059	3.31
40	0.28	3.13	0.045	3.44
45	0.20	2.95	0.035	3.50
50	0.14	2.80	0.027	3.53
55	0.11	2.54	0.022	3.39
60	0.08	2.32	0.017	3.22
70	0.05	1.91	0.012	2.78
100	0.018	1.10	0.005	1.69
150	0.005	0.73	0.0015	1.42
200	0.002	0.55	0.0006	1.21
>200	$1.81 \times 10^4 E^{-3}$	$110E^{-1}$	$4.8 \times 10^3 E^{-3}$	$(-298 + 102 \ln E)/E$

constructing a cross-section profile versus electron-impact energy for the $O(^3P \to 3p\,^5P)$ transition. This is shown in Fig. 5; values are given in Table 5. For energies > 30 eV the following approximation is used:

$$\sigma(E) = (1.81 \times 10^{-14} \text{ cm}^2 \text{ eV}^3)E^{-3}. \qquad (8)$$

Gulcicek et al. (1988) and Gulcicek and Doering (1987) also report direct measurements of the $O(^3P \to 3p\,^3P)$ cross section in the 13.87–100 eV range. Gulcicek et al. write that optical data of E. C. Zipf, which include experimentally determined corrections for cascading, support these measurements for electron-impact energies > 30 eV (from a private communication between Gulcicek et al. and E. C. Zipf). The theoretical cross section of Julienne and Davis (1976) at 20 eV is 26% less in magnitude than the latest measurement. The semi-empirical cross section of Dalgarno and Lejuene (1971) is about a factor of 10 lower than the new measurements.

Figure 5 and Table 5 give the recommended values for the $O(^3P \to 3p\,^3P)$ cross section, based on the experimental results. For $E > 100$ eV,

$$\sigma(E) = (1.10 \times 10^{-16} \text{ cm}^2 \text{ eV})E^{-1} \qquad (9)$$

is a valid approximation for this electric quadrupole transition.

2.3.d. $O(^3P \to 3d\,^5D^o, 3d\,^3D^o)$

No experimental data on the $O(^3P \to 3d\,^5D^o)$ cross section as a function of electron-impact energy are available, as is the case for many of the atomic oxygen Rydberg states. We therefore use Eq. (2), with $W = 12.07$ eV, $\alpha = 1$, $\beta = 2$, $\Omega = 3$, and $F = 0.2/(3 - 0.01)^3 = 0.007$ (Jackman et al., 1977), and $\gamma = 0$. This cross section is plotted in Fig. 5;

Table 6. $O(^3P \to 4s\,^5S^o, 4s\,^3S^o)$ excitation cross sections.

Electron energy (eV)	σ (10^{-18} cm^2)	
	$4s\,^5S^o$	$4s\,^3S^o$
11.9	0.01	-
12	0.02	0.04
12.1	0.03	0.19
12.5	0.11	1.20
13	0.34	1.54
14	0.46	1.68
16	0.57	1.79
18	0.64	1.86
20	0.62	1.89
25	0.46	1.77
28	0.35	1.58
30	0.30	1.48
35	0.18	1.42
40	0.12	1.38
45	0.09	1.35
50	0.06	1.33
55	0.05	1.30
60	0.04	1.27
70	0.02	1.22
100	0.01	1.07
150	0.002	0.90
200	0.0009	0.74
>200	$7.5 \times 10^3 E^{-3}$	$(-148 + 56 \ln E)/E$

corresponding values are given in Table 5.

Recent measurements of the $O(^3P \to 3d\,^3D^o)$ excitation cross section at electron-impact energies of 30, 50, and 100 eV, by the method of electron energy loss, are reported by Vaughan and Doering (1988). Their results agree with the optical cross sections of Zipf and Erdman (1985) within experimental error except at energies greater than ~ 80 eV where Vaughan and Doering's data fall off more rapidly with increasing energy. Vaughan and Doering suggest that this is because cascade contributions in the optical measurements become progressively more important at higher energies; they do not, however, speculate on the identities of the cascade states. Zipf and Erdman, on the other hand, point out that their optical cross sections probably contain cascade contributions from $nf\,^3F$ states which may be significant below 50 eV.

We have decided to adopt the measurements of Vaughan and Doering (1988) for the $O(^3P \to 3d\,^3D^o)$ cross section. The cross section is shown in Fig. 5, and values are tabulated in Table 5. For electron-impact energies > 100 eV we approximate the cross section using Eq. (3) with $F = 0.019$ (Doering et al., 1985) and $A = -2.98 \times 10^{-16}$ cm^2 eV.

2.3.e. Transitions to $O^+(^4S^o)$-Core Rydberg States with $n = 4$

For excitation to the $4s\,^5S^o$ Rydberg state the quantum defect method outlined in Sec. 2.2 is used. We find that this cross section is 20% of the $3s\,^5S^o$ cross section. The $O(^3P \to 4s\,^5S^o)$ cross section is given in Fig. 6 and Table 6.

FIG. 6. $O(^3P \to 4s\,^5S^o, 4s\,^3S^o)$ excitation cross sections.
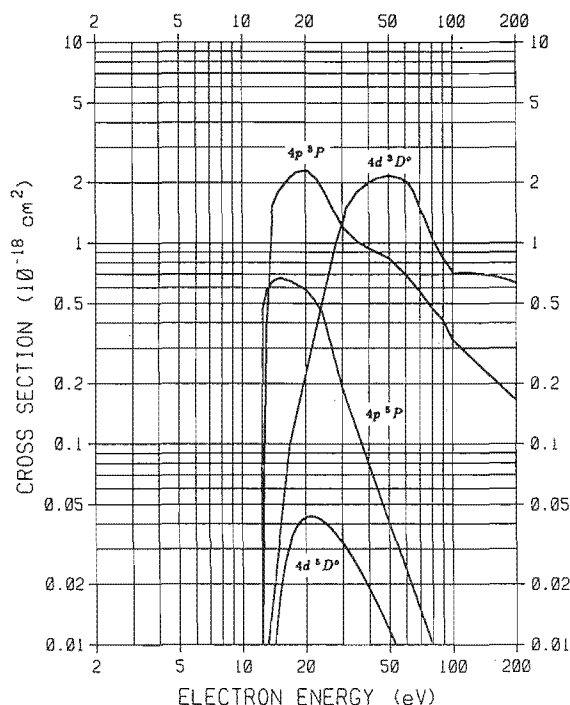
FIG. 7. $O(^3P \to 4p\ ^5P, 4p\ ^3P, 4d\ ^5D^\circ, 4d\ ^3D^\circ)$ excitation cross sections.

We scale the $O(^3P \to 3s\ ^3S^\circ)$ cross section by

$$\frac{W_3 F_4}{W_4 F_3} = \frac{(9.51\ \text{eV})(0.01)}{(11.92\ \text{eV})(0.048)} = 0.17 \qquad (10)$$

in order to obtain the $O(^3P \to 4s\ ^3S^\circ)$ cross section, where the optical oscillator strengths, F_3 and F_4 for the $n = 3$ and $n = 4$ states, respectively, have been measured by Doering *et al.* (1985). Note that if we had used Eq. (5) instead of the measured value for F_4, the required scale factor would be overestimated by 28%, thus indicating the limitations of the quantum defect method for this transition. Values for this cross section as a function of electron energy are given in Fig. 6 and Table 6.

The excitation cross section for the $4p\ ^5P$ Rydberg state is calculated using Eqs. (4) and (5). This cross section is 28% of the $3p\ ^5P$ cross section. The results are given in Fig. 7 and Table 7.

Equations (4) and (5) are also used to obtain the cross sections for the $4p\ ^3P$ Rydberg state from the $n = 3$ cross section. Accordingly, the scale factor is 0.30. This cross section is shown in Fig. 7 and listed in Table 7.

The $O(^3P \to 4d\ ^5D^\circ)$ cross section is obtained using Eq. (2), with $W = 12.74$ eV, $\alpha = 1, \beta = 2, \Omega = 3$, and $F = 0.2/(4 - 0.01)^3 = 0.003$ (Jackman *et al.*, 1977), and $\gamma = 0$. This cross section is plotted in Fig. 7; corresponding values are given in Table 7.
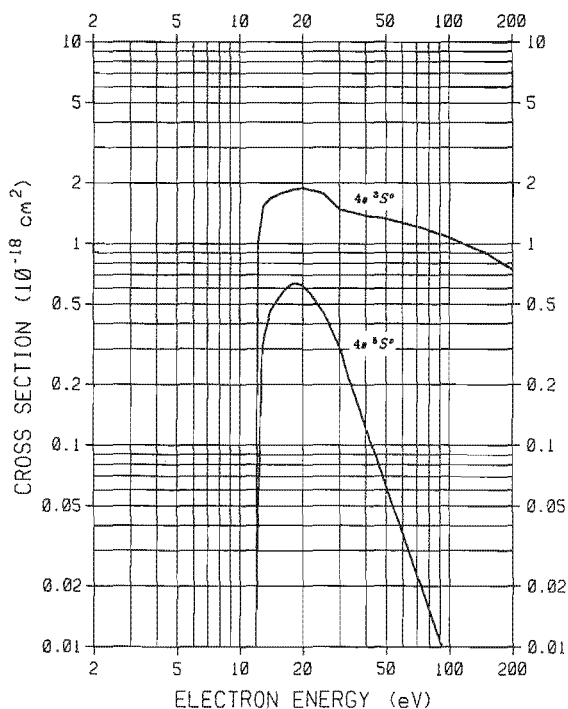
Table 7. $O(^3P \longrightarrow 4p\ ^5P, 4p\ ^3P, 4d\ ^5D^\circ, 4d\ ^3D^\circ)$ excitation cross sections.

Electron energy (eV)	$\sigma\ (10^{-18}\ \text{cm}^2)$			
	$4p\ ^5P$	$4p\ ^3P$	$4d\ ^5D^\circ$	$4d\ ^3D^\circ$
12.5	0.48	0.02	-	-
12.7	0.52	0.07	-	-
12.9	0.56	0.20	0.00019	-
13	0.59	0.36	0.0005	-
13.5	0.62	0.84	0.0034	0.01
14	0.65	1.57	0.008	0.02
15	0.67	1.83	0.018	0.03
16	0.66	1.99	0.026	0.06
17	0.64	2.14	0.033	0.11
18	0.62	2.26	0.038	0.14
20	0.59	2.31	0.043	0.22
22	0.52	2.14	0.043	0.34
25	0.38	1.74	0.040	0.62
28	0.25	1.37	0.035	1.03
30	0.19	1.20	0.032	1.29
35	0.12	1.02	0.025	1.78
40	0.08	0.94	0.019	2.00
45	0.06	0.89	0.015	2.12
50	0.04	0.84	0.012	2.17
55	0.03	0.76	0.009	2.12
60	0.02	0.70	0.008	2.03
70	0.01	0.57	0.005	1.50
100	0.01	0.33	0.002	0.72
150	0.0015	0.22	0.0007	0.69
200	0.0006	0.17	0.0003	0.64
>200	$5.1 \times 10^3 E^{-3}$	$33E^{-1}$	$2.4 \times 10^3 E^{-3}$	$(-306 + 82 \ln E)/E$

Excitation cross-section measurements of the $O(^3P \to nd\ ^3D^o)$ Rydberg transitions for $n = 4$, 5, and 6 have been made at 30, 50, and 100 eV, and the cross section for the $O(^3P \to 7d\ ^3D^o)$ transition has been measured at 100 eV (Vaughan and Doering, 1988). The $n \geqslant 4$ profiles of cross section versus electron-impact energy are of similar shape, and are distinctly more sharply peaked than the $n = 3$ case (see Sec. 2.3.d.). We therefore fit a curve to the $n = 4$ data (see Fig. 7 and Table 7), and assume that its shape will be the same for all higher Rydberg transitions in this series. From the optical oscillator strength $F_4 = 0.016$ (Doering et al., 1985), the corresponding energy threshold (given in Table 1), and the measurement at 100 eV, the $n = 4$ cross section for electron energies greater than 100 eV can be approximated using Eq. (3) with $A = -3.06 \times 10^{-16}$ cm^2 eV.

2.3.f. Transitions to $O^+(^4S^o)$-Core Rydberg States with $n \geqslant 5$

For excitations to the $n \geqslant 5$ states of the $ns\ ^5S^o$ Rydberg series, Eq. (6) requires that the $\Sigma n \geqslant 5$ cross section is 18% of the $3s\ ^5S^o$ cross section. This cross section is given in Fig. 8 and Table 8.

For the sum of the cross sections of the $n \geqslant 5$ states in the $ns\ ^3S^o$ Rydberg series, we scale the $O(^3P \to 4s\ ^3S^o)$ cross section by

Table 8. $O(^3P \longrightarrow \Sigma(n \geq 5)\ ns\ ^5S^o, \Sigma(n \geq 5)\ ns\ ^3S^o)$ excitation cross sections.

Electron energy (eV)	$\sigma\ (10^{-18}\ \text{cm}^2)$	
	$\Sigma(n \geq 5)\ ns\ ^5S^o$	$\Sigma(n \geq 5)\ ns\ ^3S^o$
13.4	0.10	0.04
13.6	0.31	0.14
13.8	0.36	0.45
14	0.40	1.04
15	0.46	1.49
16	0.51	1.61
17	0.55	1.67
18	0.57	1.73
19	0.57	1.74
20	0.56	1.76
22	0.50	1.71
25	0.41	1.64
28	0.32	1.47
30	0.27	1.37
35	0.16	1.32
40	0.11	1.28
45	0.08	1.26
50	0.06	1.23
55	0.04	1.20
60	0.03	1.18
70	0.02	1.13
100	0.01	1.00
150	0.002	0.83
200	0.0009	0.69
>200	$7.5 \times 10^3 E^{-3}$	$(-137 + 52\ \ln E)/E$

FIG. 9. $O(^3P \to \Sigma(n \geqslant 5) \; np \; ^5P, \Sigma(n \geqslant 5) \; np \; ^3P, \Sigma(n \geqslant 5) \; nd \; ^5D^o, \Sigma(n \geqslant 5)$ $nd \; ^3D^o)$ excitation cross sections.

$$\frac{W_4(4-\delta)^3}{2W_A(4.5-\delta)^2} = \frac{(11.92 \text{ eV})(4-1.16)^3}{2(13.15 \text{ eV})(4.5-1.16)^2} = 0.93.$$

(11)

Values for this cross section as a function of electron energy are given in Fig. 8 and Table 8.

The sum of the cross sections for the $n \geqslant 5$ states of the $np \; ^5P$ Rydberg series is calculated using Eq. (6). It is found to be 31% of the $3p \; ^5P$ cross section. This cross section is graphed in Fig. 9 and tabulated in Table 9.

From Eq. (6), we find that the composite cross section for the $n \geqslant 5$ states of the $np \; ^3P$ Rydberg series is 35% of the $3p \; ^3P$ cross section. The $\Sigma n \geqslant 5$ cross section for this series is given in Fig. 9 and Table 9.

We obtain the $O(^3P \to \Sigma(n \geqslant 5)nd \; ^5D^o)$ cross section using Eq. (2), with $W = 13.33$ eV from Table 1, $\alpha = 1$, $\beta = 2$, $\Omega = 3$, and $F = 0.2/[2(4.5-0.01)^2] = 0.005$ (Jackman et al., 1977), and $\gamma = 0$. The expression for F is consistent with the quantum defect method discussed in Sec. 2.2. This cross section is plotted in Fig. 9; corresponding values are given in Table 9.

For $\sigma_{n>5}(E)$ of the $nd \; ^3D^o$ Rydberg series, we scale the $4d \; ^3D^o$ data using an equation similar to Eq. (6):

Table 9. $O(^3P \longrightarrow \Sigma(n \geq 5) \; np \; ^5P, \Sigma(n \geq 5) \; np \; ^3P, \Sigma(n \geq 5) \; nd \; ^5D^o, \Sigma(n \geq 5) \; nd \; ^3D^o)$ excitation cross sections.

Electron energy (eV)	$\sigma \; (10^{-18} \; \text{cm}^2)$			
	$\Sigma(n \geq 5) \; np \; ^5P$	$\Sigma(n \geq 5) \; np \; ^3P$	$\Sigma(n \geq 5) \; nd \; ^5D^o$	$\Sigma(n \geq 5) \; nd \; ^3D^o$
13.4	0.07	0.04	-	-
13.6	0.25	0.18	0.0007	-
13.8	0.40	0.82	0.0019	0.01
14	0.62	1.48	0.0036	0.02
15	0.69	2.13	0.016	0.04
16	0.70	2.32	0.029	0.08
17	0.71	2.50	0.041	0.16
18	0.69	2.63	0.050	0.21
19	0.67	2.66	0.056	0.26
20	0.65	2.70	0.060	0.33
22	0.58	2.49	0.063	0.52
25	0.43	2.03	0.060	0.92
28	0.27	1.60	0.054	1.54
30	0.21	1.40	0.049	1.94
35	0.13	1.19	0.039	2.67
40	0.09	1.10	0.030	3.00
45	0.06	1.03	0.023	3.17
50	0.04	0.98	0.019	3.26
55	0.03	0.89	0.015	3.18
60	0.03	0.81	0.012	3.05
70	0.02	0.67	0.008	2.25
100	0.01	0.38	0.003	1.08
150	0.0017	0.26	0.0011	1.04
200	0.0007	0.195	0.00047	0.95
>200	$5.6 \times 10^3 E^{-3}$	$39E^{-1}$	$3.76 \times 10^3 E^{-3}$	$(-461 + 123 \ln E)/E$

FIG. 10. O($^3P\rightarrow 3s'$ $^3D^o$, $3s'$ $^1D^o$, $3p'$ ^3PDF, $3p'$ ^1PDF) excitation cross sections.

$$\sigma_{n\geqslant 5}(E) = \sum_{n=5}^{\infty} \sigma_n(E) = \frac{W_4(4-\delta)^3}{2W_A(4.5-\delta)^2}\sigma_4(E)$$

$$= \frac{(12.75 \text{ eV})(4-0.01)^3}{2(13.33 \text{ eV})(4.5-0.01)^2}\sigma_4(E)$$

$$\approx (1.5)\sigma_4(E). \qquad (12)$$

The data show that this method of approximation gives cross sections within experimental error up to $n = 7$ in the series. Figure 9 and Table 9 give the recommended values for this cross section.

2.4. Transitions to Rydberg States with an O$^+(2s^22p^3$ $^2D^o)$ Core

2.4.a. O($^3P\rightarrow 3s'$ $^3D^o$, $3s'$ $^1D^o$, $3p'$ ^3PDF, $3p'$ ^1PDF)

Electron energy-loss measurements of the O($^3P\rightarrow 3s'$ $^3D^o$) excitation cross section have been made by Vaughan and Doering (1987) and Gulcicek and Doering (1988) in the 20–200 eV range. In the latter work, a new value for the electron-impact cross section at 20 eV, measured following improvements to the experimental apparatus for near-threshold energies, is reported which replaces the 20 and 25 eV values of the former work. These data are a

Table 10. O($^3P \longrightarrow 3s'$ $^3D^o$, $3s'$ $^1D^o$, $3p'$ ^3PDF, $3p'$ ^1PDF) excitation cross sections.

Electron energy (eV)	σ (10^{-18} cm^2)			
	$3s'$ $^3D^o$	$3s'$ $^1D^o$	$3p'$ ^3PDF	$3p'$ ^1PDF
13	0.05	0.006	-	-
13.5	0.24	0.037	-	-
14	1.08	0.080	-	-
14.5	2.47	0.135	-	0.024
15	3.56	0.187	-	0.057
16	5.10	0.28	0.144	0.099
17	5.52	0.35	0.399	0.120
18	5.61	0.40	0.586	0.130
19	5.50	0.43	0.722	0.132
20	5.41	0.45	0.822	0.130
22	5.09	0.46	0.945	0.120
25	4.88	0.42	1.019	0.099
28	4.95	0.37	1.026	0.081
30	5.07	0.34	1.013	0.070
35	5.64	0.26	0.953	0.050
40	5.85	0.20	0.882	0.036
45	5.98	0.154	0.813	0.027
50	5.87	0.122	0.751	0.021
55	5.58	0.097	0.695	0.016
60	5.33	0.079	0.646	0.013
70	4.93	0.053	0.564	0.008
100	4.48	0.021	0.406	0.003
150	4.00	0.007	0.274	0.001
200	2.67	0.003	0.207	0.0004
>200	$(-1145+317\ln E)/E$	$2.4\times10^4 E^{-3}$	$41.4E^{-1}$	$3.3\times10^3 E^{-3}$

factor of 3 lower than the optical cross sections reported by Zipf and Erdman (1985); however, the profile shapes are similar. Vaughan and Doering write that, based on the assumption that cascade contributions to the optical cross sections of Zipf and Erdman are 25% or less, a reduction in the Zipf and Erdman values by a factor of 2 would be needed to make the values consistent with their own measurements. As a result of their analysis of mid-latitude dayglow data obtained from rocket measurements, Gladstone et al. (1987) came to the similar conclusion that the Zipf and Erdman values should be reduced by a factor of ~2–3 in order to explain their observations using the 1173-Å/989-Å branching ratio measured by Morrison (1985) and Erdman and Zipf (1986). In addition Gladstone et al. (1987) also cite other airglow studies, over a wide range of aeronomical conditions, that also require a reduction in the Zipf and Erdman cross sections to bring the models into agreement with the observations. Note that Meier (1982) required a cross section of 8.4×10^{-18} cm^2 at 25 eV in order to explain rocket observations of the 989-Å dayglow under optically thick conditions, but this was based on a model value of the 7990-Å/989-Å branching ratio shown later by Erdman and Zipf (1983) to be too large by more than an order of magnitude.

We therefore recommend that the new measurements be used. A hand interpolation of the data from threshold to 200 eV is shown in Fig. 10, and numerical values are tabulated in Table 10. For $E > 200$ eV the cross section is approximated by Eq. (3) with $F = 0.061$ (Doering et al., 1985) and $A = -1.145 \times 10^{-15}$ cm^2 eV.

No measured cross sections for transitions to the $3s'$ $^1D^o$, $3p'$ ^3PDF, and $3p'$ ^1PDF states (where the P, D, and F cross sections for a given spin have been added due to their similar thresholds and theoretical high-energy behaviors, resulting in a composite PDF cross section) are available. However, Jackman et al. (1977) have estimated values for these excitations which can be calculated using Eq. (2) (with $\gamma = 0$). For $3s'$ $^1D^o$, $W = 12.72$ eV, $\alpha = 1$, $\beta = 2$, $\Omega = 3$, and $F = 0.2/(3 - 1.18)^3 = 0.033$. For $3p'$ ^3PDF, $W = 14.06$ eV, $\alpha = 2$, $\beta = 1$, $\Omega = 1$, and $F = 0.1/(3 - 0.84)^3 = 0.01$. And for $3p'$ ^1PDF, $W = 14.20$ eV, $\alpha = 1$, $\beta = 1$, $\Omega = 3$, and $F = 0.04/(3 - 0.83)^3 = 0.004$. These cross sections are plotted in Fig. 10 and listed in Table 10.

2.4.b. O($^3P \rightarrow 3d'$ $^3S^o$, $3d'$ $^3P^o$, $3d'$ $^3D^o$, $3d'$ $^3FG^o$, $3d'$ $^1SPDFG^o$)

There are currently no measured cross sections available for excitation to the $3d'$ $^3S^o$, $3d'$ $^3P^o$, and $3d'$ $^3D^o$ states; however, Vaughan and Doering (1988) have measured the O($^3P \rightarrow 4d'$ $^3P^o$) cross section using the electron energy-loss method. We make the assumption that the O($^3P \rightarrow 3d'$ $^3P^o$) cross section is related to the O($^3P \rightarrow 4d'$ $^3P^o$) cross section by a scale factor. Then using the quantum defect method (as explained in Sec. 2.2) and the quantum defect $\delta = 0.04$ given by Jackman et al. (1977) for this Rydberg series, the scale factor is given by

$$\frac{W_4(4 - \delta)^3}{W_3(3 - \delta)^3} = \frac{(16.08 \text{ eV})(4 - 0.04)^3}{(15.36 \text{ eV})(3 - 0.04)^3} = 2.51, \quad (13)$$

where W_3 and W_4 are the threshold energies for the $n = 3$

FIG. 11. O($^3P \rightarrow 3d'$ $^3S^o$, $3d'$ $^3P^o$, $3d'$ $^3D^o$, $3d'$ $^3FG^o$, $3d'$ $^1SPDFG^o$) excitation cross sections.

and $n = 4$ states, respectively, given in Table 1. The O($^3P \rightarrow 3d'$ $^3P^o$) cross section is presented in Fig. 11 and in Table 11 as a function of electron-impact energy. For $E > 200$ eV the O($^3P \rightarrow 3d'$ $^3P^o$) cross section is approximated by letting $F = 0.0077$ (Jackman et al., 1977) and $A = 2.71 \times 10^{-16}$ cm^2 eV in Eq. (3). We furthermore make the assumption that $^3S^o$ and $^3D^o$ cross sections are related to the $^3P^o$ cross section by scale factors, and use the optical oscillator strengths 0.0065 and 0.0052 for the $^3S^o$ and $^3D^o$ states, respectively (Jackman et al., 1977), as relative weights. The resulting $^3S^o$ and $^3D^o$ cross sections are also plotted in Fig. 11, with corresponding values presented in Table 11.

No measured cross sections have been reported for transitions to the $3d'$ $^3FG^o$ and $3d'$ $^1SPDFG^o$ states. The estimates of Jackman et al. (1977) are therefore used, namely, Eq. (2) (with $\gamma = 0$) and the following parameters: for $3d'$ $^3FG^o$, $W = 15.39$ eV, $\alpha = 2$, $\beta = 1$, $\Omega = 1$, and $F = 0.1/(3 - 0.04)^3 = 0.004$; for $3d'$ $^1SPDFG^o$, $W = 15.40$ eV, $\alpha = 1$, $\beta = 2$, $\Omega = 3$, and $F = 0.2/(3 - 0.04)^3 = 0.008$. These cross sections are plotted in Fig. 11 and listed in Table 11.

2.4.c. Transitions to O$^+$ ($^2D^o$)-Core Rydberg States with $n = 4$

The O($^3P \rightarrow 4s'$ $^3D^o$) cross section is obtained using Eqs. (4) and (5), and data from Tables 1 and 2; it is found to be 22% of the O($^3P \rightarrow 3s'$ $^3D^o$) cross section. The results are presented in Fig. 12 and Table 12.

The cross sections for transitions to the $4s'$ $^1D^o$, $4p'$ ^3PDF, and $4p'$ ^1PDF states are obtained from the estimates of Jackman et al. (1977). We therefore use Eq. (2)

factor of 3 lower than the optical cross sections reported by Zipf and Erdman (1985); however, the profile shapes are similar. Vaughan and Doering write that, based on the assumption that cascade contributions to the optical cross sections of Zipf and Erdman are 25% or less, a reduction in the Zipf and Erdman values by a factor of 2 would be needed to make the values consistent with their own measurements. As a result of their analysis of mid-latitude dayglow data obtained from rocket measurements, Gladstone et al. (1987) came to the similar conclusion that the Zipf and Erdman values should be reduced by a factor of ~2–3 in order to explain their observations using the 1173-Å/989-Å branching ratio measured by Morrison (1985) and Erdman and Zipf (1986). In addition Gladstone et al. (1987) also cite other airglow studies, over a wide range of aeronomical conditions, that also require a reduction in the Zipf and Erdman cross sections to bring the models into agreement with the observations. Note that Meier (1982) required a cross section of 8.4×10^{-18} cm^2 at 25 eV in order to explain rocket observations of the 989-Å dayglow under optically thick conditions, but this was based on a model value of the 7990-Å/989-Å branching ratio shown later by Erdman and Zipf (1983) to be too large by more than an order of magnitude.

We therefore recommend that the new measurements be used. A hand interpolation of the data from threshold to 200 eV is shown in Fig. 10, and numerical values are tabulated in Table 10. For $E > 200$ eV the cross section is approximated by Eq. (3) with $F = 0.061$ (Doering et al., 1985) and $A = -1.145 \times 10^{-15}$ cm^2 eV.

No measured cross sections for transitions to the $3s'$ $^1D^o$, $3p'$ ^3PDF, and $3p'$ ^1PDF states (where the P, D, and F cross sections for a given spin have been added due to their similar thresholds and theoretical high-energy behaviors, resulting in a composite PDF cross section) are available. However, Jackman et al. (1977) have estimated values for these excitations which can be calculated using Eq. (2) (with $\gamma = 0$). For $3s'$ $^1D^o$, $W = 12.72$ eV, $\alpha = 1$, $\beta = 2$, $\Omega = 3$, and $F = 0.2/(3 - 1.18)^3 = 0.033$. For $3p'$ ^3PDF, $W = 14.06$ eV, $\alpha = 2$, $\beta = 1$, $\Omega = 1$, and $F = 0.1/(3 - 0.84)^3 = 0.01$. And for $3p'$ ^1PDF, $W = 14.20$ eV, $\alpha = 1$, $\beta = 1$, $\Omega = 3$, and $F = 0.04/(3 - 0.83)^3 = 0.004$. These cross sections are plotted in Fig. 10 and listed in Table 10.

2.4.b. O($^3P \rightarrow 3d'$ $^3S^o$, $3d'$ $^3P^o$, $3d'$ $^3D^o$, $3d'$ $^3FG^o$, $3d'$ $^1SPDFG^o$)

There are currently no measured cross sections available for excitation to the $3d'$ $^3S^o$, $3d'$ $^3P^o$, and $3d'$ $^3D^o$ states; however, Vaughan and Doering (1988) have measured the O($^3P \rightarrow 4d'$ $^3P^o$) cross section using the electron energy-loss method. We make the assumption that the O($^3P \rightarrow 3d'$ $^3P^o$) cross section is related to the O($^3P \rightarrow 4d'$ $^3P^o$) cross section by a scale factor. Then using the quantum defect method (as explained in Sec. 2.2) and the quantum defect $\delta = 0.04$ given by Jackman et al. (1977) for this Rydberg series, the scale factor is given by

$$\frac{W_4(4 - \delta)^3}{W_3(3 - \delta)^3} = \frac{(16.08 \text{ eV})(4 - 0.04)^3}{(15.36 \text{ eV})(3 - 0.04)^3} = 2.51, \quad (13)$$

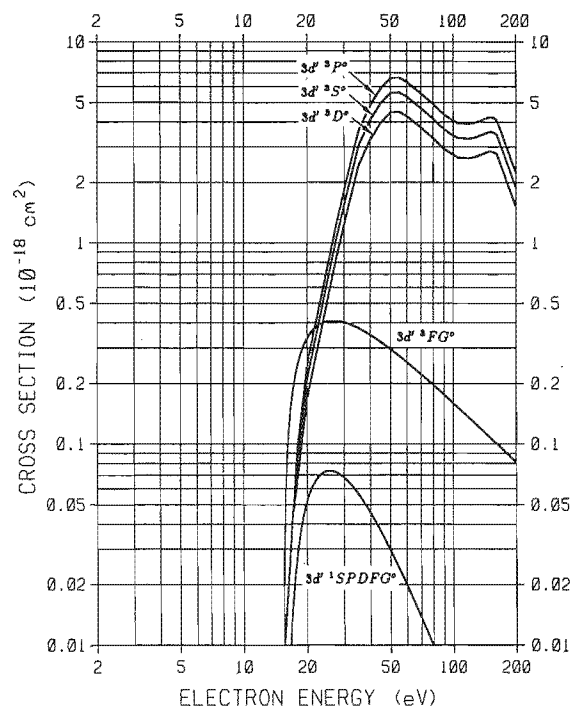where W_3 and W_4 are the threshold energies for the $n = 3$

FIG. 11. O($^3P \rightarrow 3d'$ $^3S^o$, $3d'$ $^3P^o$, $3d'$ $^3D^o$, $3d'$ $^3FG^o$, $3d'$ $^1SPDFG^o$) excitation cross sections.

and $n = 4$ states, respectively, given in Table 1. The O($^3P \rightarrow 3d'$ $^3P^o$) cross section is presented in Fig. 11 and in Table 11 as a function of electron-impact energy. For $E > 200$ eV the O($^3P \rightarrow 3d'$ $^3P^o$) cross section is approximated by letting $F = 0.0077$ (Jackman et al., 1977) and $A = 2.71 \times 10^{-16}$ cm^2 eV in Eq. (3). We furthermore make the assumption that $^3S^o$ and $^3D^o$ cross sections are related to the $^3P^o$ cross section by scale factors, and use the optical oscillator strengths 0.0065 and 0.0052 for the $^3S^o$ and $^3D^o$ states, respectively (Jackman et al., 1977), as relative weights. The resulting $^3S^o$ and $^3D^o$ cross sections are also plotted in Fig. 11, with corresponding values presented in Table 11.

No measured cross sections have been reported for transitions to the $3d'$ $^3FG^o$ and $3d'$ $^1SPDFG^o$ states. The estimates of Jackman et al. (1977) are therefore used, namely, Eq. (2) (with $\gamma = 0$) and the following parameters: for $3d'$ $^3FG^o$, $W = 15.39$ eV, $\alpha = 2$, $\beta = 1$, $\Omega = 1$, and $F = 0.1/(3 - 0.04)^3 = 0.004$; for $3d'$ $^1SPDFG^o$, $W = 15.40$ eV, $\alpha = 1$, $\beta = 2$, $\Omega = 3$, and $F = 0.2/(3 - 0.04)^3 = 0.008$. These cross sections are plotted in Fig. 11 and listed in Table 11.

2.4.c. Transitions to O$^+$ ($^2D^o$)-Core Rydberg States with $n = 4$

The O($^3P \rightarrow 4s'$ $^3D^o$) cross section is obtained using Eqs. (4) and (5), and data from Tables 1 and 2; it is found to be 22% of the O($^3P \rightarrow 3s'$ $^3D^o$) cross section. The results are presented in Fig. 12 and Table 12.

The cross sections for transitions to the $4s'$ $^1D^o$, $4p'$ ^3PDF, and $4p'$ ^1PDF states are obtained from the estimates of Jackman et al. (1977). We therefore use Eq. (2)

Table 11. O($^3P \longrightarrow 3d'\ ^3S^o$, $3d'\ ^3P^o$, $3d'\ ^3D^o$, $3d'\ ^3FG^o$, $3d'\ ^1SPDFG^o$) excitation cross sections.

Electron energy (eV)	σ (10^{-18} cm^2)				
	$3d'\ ^3S^o$	$3d'\ ^3P^o$	$3d'\ ^3D^o$	$3d'\ ^3FG^o$	$3d'\ ^1SPDFG^o$
15.8	0.01	0.01	0.01	0.052	0.0012
16	0.02	0.02	0.02	0.075	0.003
17	0.04	0.04	0.04	0.171	0.014
18	0.08	0.10	0.07	0.24	0.027
19	0.14	0.16	0.11	0.29	0.040
20	0.21	0.25	0.17	0.33	0.050
22	0.34	0.41	0.27	0.37	0.064
25	0.65	0.78	0.52	0.40	0.072
28	1.15	1.36	0.92	0.40	0.070
30	1.57	1.86	1.26	0.395	0.067
35	3.02	3.58	2.42	0.37	0.056
40	4.10	4.86	3.28	0.34	0.045
45	4.98	5.90	3.98	0.32	0.036
50	5.57	6.60	4.46	0.29	0.029
55	5.62	6.65	4.49	0.27	0.024
60	5.34	6.33	4.27	0.25	0.020
70	4.68	5.54	3.74	0.22	0.0135
100	3.42	4.06	2.74	0.157	0.0055
150	3.57	4.23	2.86	0.106	0.0018
200	1.87	2.22	1.50	0.080	0.0008
>200	$(229 + 27.5 \ln E)/E$		$(183 + 22.0 \ln E)/E$		$6.4 \times 10^3 E^{-3}$
	$(271 + 32.6 \ln E)/E$		$16.0 E^{-1}$		

(with $\gamma = 0$) and the following: for $4s'\ ^1D^o$, $W = 15.22$ eV, $\alpha = 1, \beta = 2, \Omega = 3$, and $F = 0.2/(4 - 1.18)^3 = 0.009$; for $4p'\ ^3PDF$, $W = 15.59$ eV, $\alpha = 2$, $\beta = 1$, $\Omega = 1$, and $F = 0.1/(4 - 0.84)^3 = 0.003$; and for $3p'\ ^1PDF$, $W = 15.58$ eV, $\alpha = 1$, $\beta = 1$, $\Omega = 3$, and $F = 0.04/(4 - 0.83)^3 = 0.0013$. These cross sections are plotted in Fig. 12 and listed in Table 12.

Vaughan and Doering (1988) have measured the O($^3P \to 4d'\ ^3P^o$) cross section at 30, 50, 100, 150, and 200 eV, using the electron energy-loss method. As done in Sec. 2.4.b. the relative optical oscillator strengths for the $nd'\ ^3S^o$, $nd'\ ^3P^o$, and $nd'\ ^3D^o$ states given by Jackman et al. (1977) are used to determine the magnitudes of the O($^3P \to 4d'\ ^3S^o$) and O($^3P \to 4d'\ ^3D^o$) cross sections, under the assumption that the variation of the cross section with electron energy is the same for all three series. In Fig. 13 and Table 13 values for the summed O($^3P \to 4d'\ ^3SPD^o$) cross section are presented. For $E > 200$ eV this total cross section is given by Eq. (3) with $F = 0.008$ (Jackman et al., 1977) and $A = 2.72 \times 10^{-16}$ cm^2 eV.

Using Eq. (2) (with $\gamma = 0$), the $4d'\ ^3FG^o$ cross section is obtained with $W = 16.07$ eV, $\alpha = 2$, $\beta = 1$, $\Omega = 1$, and $F = 0.1/(4 - 0.04)^3 = 0.0016$, and the $4d'\ ^1SPDFG^o$ cross section is obtained with $W = 16.07$, $\alpha = 1$, $\beta = 2$, $\Omega = 3$, and $F = 0.2/(4 - 0.04)^3 = 0.0032$ (Jackman et al., 1977).
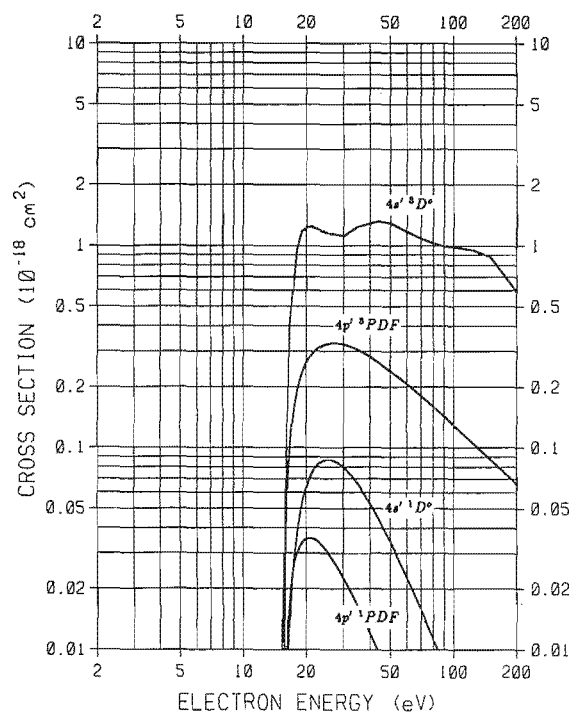
FIG. 12. O($^3P \to 4s'\ ^3D^o$, $4s'\ ^1D^o$, $4p'\ ^3PDF$, $4p'\ ^1PDF$) excitation cross sections.

Table 12. $O(^3P \longrightarrow 4s'\ ^3D^o, 4s'\ ^1D^o, 4p'\ ^3PDF, 4p'\ ^1PDF)$ excitation cross sections.

Electron energy (eV)	σ $(10^{-18}$ cm$^2)$			
	$4s'\ ^3D^o$	$4s'\ ^1D^o$	$4p'\ ^3PDF$	$4p'\ ^1PDF$
15.5	0.02	0.0008	-	-
16	0.09	0.0051	0.042	0.0082
16.5	0.33	0.012	0.086	0.016
17	0.52	0.020	0.124	0.022
18	0.95	0.036	0.184	0.029
19	1.17	0.051	0.228	0.034
20	1.23	0.063	0.260	0.035
22	1.22	0.079	0.300	0.035
25	1.15	0.086	0.324	0.031
28	1.13	0.084	0.326	0.026
30	1.12	0.079	0.322	0.023
35	1.24	0.066	0.303	0.017
40	1.29	0.053	0.281	0.012
45	1.32	0.042	0.259	0.0091
50	1.29	0.034	0.239	0.0070
55	1.23	0.028	0.221	0.0055
60	1.17	0.023	0.206	0.0043
70	1.08	0.016	0.180	0.0029
100	0.99	0.0063	0.129	0.0010
150	0.88	0.0021	0.087	0.00034
200	0.59	0.0009	0.066	0.00015
>200	$(-253 + 70 \ln E)/E$	$7.5 \times 10^3 E^{-3}$	$13.2E^{-1}$	$1.2 \times 10^3 E^{-3}$

FIG. 13. $O(^3P \to 4d'\ ^3SPD^o, 4d'\ ^3FG^o, 4d'\ ^1SPDFG^o)$ excitation cross sections.

TABLE 13. $O(^3P \to 4d'\ ^3SPD^o, 4d'\ ^3FG^o, 4d'\ ^1SPDFG^o)$ excitation cross sections.

Electron energy (eV)	σ $(10^{-18}$ cm$^2)$		
	$4d'\ ^3SPD^o$	$4d'\ ^3FG^o$	$4d'\ ^1SPDFG^o$
16.2	-	0.008	-
16.4	0.01	0.018	-
16.8	0.02	0.035	0.001
17	0.03	0.043	0.002
18	0.10	0.075	0.007
19	0.16	0.099	0.012
20	0.25	0.117	0.017
21	0.32	0.130	0.020
22	0.41	0.139	0.023
25	0.78	0.154	0.028
28	1.36	0.157	0.028
30	1.86	0.156	0.027
35	3.58	0.148	0.023
40	4.86	0.137	0.019
45	5.90	0.127	0.015
50	6.60	0.117	0.012
55	6.65	0.109	0.010
60	6.33	0.101	0.008
70	5.54	0.089	0.006
100	4.06	0.064	0.002
150	4.23	0.043	0.001
200	2.22	0.032	0.0004
>200	$(272 + 32.4 \ln E)/E$	$6.4E^{-1}$	$3.3 \times 10^3 E^{-3}$

FIG. 14. $O(^3P \to \Sigma(n \geqslant 5)$ ns' $^3D^o$, $\Sigma(n \geqslant 5)$ ns' $^1D^o$, $\Sigma(n \geqslant 5)$ np' ^3PDF, $\Sigma(n \geqslant 5)$ np' $^1PDF)$ excitation cross sections.

These cross sections are plotted in Fig. 13 and listed in Table 13.

2.4.d. Transitions to $O^+(^2 D^o)$-Core Rydberg States with $n \geqslant 5$

The $O(^3P \to \Sigma(n \geqslant 5)ns'$ $^3D^o)$ cross section is 20% of the corresponding $n = 3$ cross section, according to Eq. (6). This cross section is given in Fig. 14 and Table 14.

The $\Sigma(n \geqslant 5)$ ns' $^1D^o$, $\Sigma(n \geqslant 5)$ np' ^3PDF, and $\Sigma(n \geqslant 5)$ np' ^1PDF cross sections are computed using Eq. (2) (with $\gamma = 0$) and the following: for ns' $^1D^o$, $W = 16.47$ eV, $\alpha = 1$, $\beta = 2$, $\Omega = 3$, and $F = 0.2/[2(4.5 - 1.18)^2] = 0.009$; for np' ^3PDF, $W = 16.54$ eV, $\alpha = 2, \beta = 1, \Omega = 1$, and $F = 0.1/[2(4.5 - 0.84)^2] = 0.0037$; and for np' ^1PDF, $W = 16.54$ eV, $\alpha = 1$, $\beta = 1$, $\Omega = 3$, and $F = 0.04/[2(4.5 - 0.83)^2] = 0.0015$ (Jackman et al., 1977). These cross sections are presented in Fig. 14 and Table 14.

The $O(^3P \to \Sigma(n \geqslant 5)nd'$ $^3SPD^o)$ cross section is obtained by multiplying the $O(^3P \to 4d'$ $^3SPD^o)$ cross section by the scale factor

$$\frac{W_4(4 - \delta)^3}{2W_4(4.5 - \delta)^2} = \frac{(16.08 \text{ eV})(4 - 0.04)^3}{2(16.65 \text{ eV})(4.5 - 0.04)^2} = 1.5;$$

$$(14)$$

Table 14. $O(^3P \longrightarrow \Sigma(n \geq 5)$ ns' $^3D^o$, $\Sigma(n \geq 5)$ ns' $^1D^o$, $\Sigma(n \geq 5)$ np' ^3PDF, $\Sigma(n \geq 5)$ np' $^1PDF)$ excitation cross sections.

Electron energy (eV)	σ $(10^{-18}$ cm$^2)$			
	$\Sigma(n \geq 5)$ ns' $^3D^o$	$\Sigma(n \geq 5)$ ns' $^1D^o$	$\Sigma(n \geq 5)$ np' ^3PDF	$\Sigma(n \geq 5)$ np' ^1PDF
16.6	0.01	-	0.010	0.002
16.8	0.02	0.001	0.030	0.006
17	0.04	0.002	0.050	0.009
18	0.51	0.013	0.130	0.023
19	0.73	0.026	0.190	0.031
20	1.04	0.039	0.235	0.035
21	1.11	0.050	0.268	0.037
22	1.10	0.058	0.293	0.037
25	1.06	0.073	0.332	0.035
28	1.02	0.075	0.343	0.030
30	1.01	0.074	0.342	0.027
35	1.11	0.064	0.327	0.020
40	1.17	0.053	0.305	0.015
45	1.20	0.043	0.283	0.011
50	1.17	0.035	0.262	0.009
55	1.12	0.029	0.244	0.007
60	1.07	0.024	0.227	0.005
70	0.99	0.017	0.199	0.004
100	0.90	0.007	0.143	0.0014
150	0.80	0.002	0.097	0.0004
200	0.53	0.001	0.073	0.00018
>200	$(-228 + 63 \ln E)/E$	$7 \times 10^3 E^{-3}$	$14.6E^{-1}$	$1.4 \times 10^3 E^{-3}$
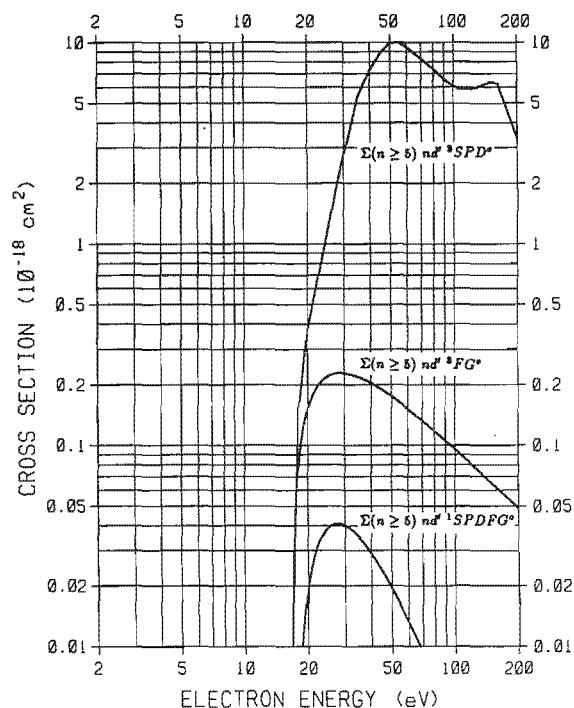
FIG. 15. O($^3P \rightarrow \Sigma(n \geqslant 5)$ nd' $^3SPD^o$, $\Sigma(n \geqslant 5)$ nd' $^3FG^o$, $\Sigma(n \geqslant 5)$ nd' $^1SPDFG^o$) excitation cross sections.

values for this cross section are given in Fig. 15 and Table 15

Using Eq. (2) (with $\gamma = 0$), the $\Sigma(n \geqslant 5)$ nd' ^3FG cross section is obtained with $W = 16.65$ eV, $\alpha = 2$, $\beta = 1$ $\Omega = 1$, and $F = 0.1/[2(4.5 - 0.04)^2] = 0.0025$, and th $\Sigma(n \geqslant 5)$ nd' $^1SPDFG^o$ cross section is obtained wit $W = 16.66$ eV, $\alpha = 1$, $\beta = 2$, $\Omega = 3$, and $F = 0.2/$ $[2(4.5 - 0.04)^2] = 0.005$ (Jackman *et al.*, 1977). These cross sections are plotted in Fig. 15 and listed in Table 15.

2.5. Transitions to Rydberg States with an O$^+$($2s^22p^3$ $^2P^o$) Core

2.5.a. O($^3P \rightarrow 3s''$ $^3P^o$, $3s''$ $^1P^o$, $3p''$ ^3SPD, $3p''$ ^1SPD)

Excitation cross sections for the O($^3P \rightarrow 3s''$ $^3P^o$) transition, measured by Vaughan and Doering (1988) using the electron energy-loss technique, are available in the 30 to 200 eV range. Upon comparison of these data with the optical cross sections of Zipf and Kao (1986) we find that the optical measurements overestimate the direct results, by a factor of ~ 2 at the peak of the cross section at 50 eV, and that the optical measurements fall off more slowly with increasing energy compared to the direct measurements. Vaughan and Doering conclude that these differences are due to cascading and perhaps other experimental difficulties as well. A reduc-

Table 15. O($^3P \longrightarrow \Sigma(n \geq 5)$ nd' $^3SPD^o$, $\Sigma(n \geq 5)$ nd' $^3FG^o$, $\Sigma(n \geq 5)$ nd' $^1SPDFG^o$) excitation cross sections.

Electron energy (eV)	σ (10^{-18} cm^2)		
	$\Sigma(n \geq 5)$ nd' $^3SPD^o$	$\Sigma(n \geq 5)$ nd' $^3FG^o$	$\Sigma(n \geq 5)$ nd' $^1SPDFG^o$
16.8	0.01	0.012	–
17	0.02	0.025	0.001
18	0.15	0.080	0.005
19	0.24	0.122	0.012
20	0.38	0.152	0.019
21	0.48	0.175	0.026
22	0.61	0.192	0.031
23	0.76	0.205	0.034
25	1.16	0.220	0.039
28	2.04	0.228	0.041
30	2.79	0.227	0.040
35	5.37	0.218	0.035
40	7.29	0.204	0.029
45	8.85	0.189	0.024
50	9.90	0.175	0.019
55	9.98	0.163	0.016
60	9.49	0.152	0.013
70	8.32	0.133	0.009
100	6.09	0.096	0.004
150	6.35	0.065	0.0009
200	3.33	0.049	0.0004
>200	$(409 + 48.5 \ln E)/E$	$9.8E^{-1}$	$3.1 \times 10^3 E^{-3}$
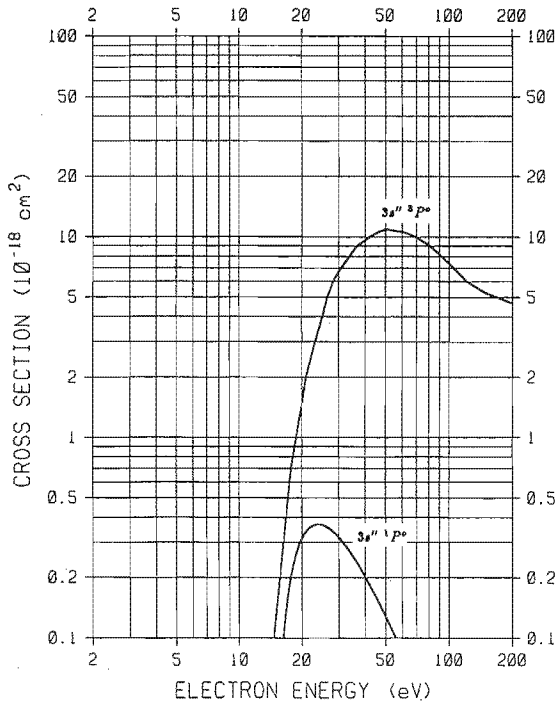
FIG. 16. O($^3P \to 3s''$ $^3P^o$, $3s''$ $^1P^o$) excitation cross sections.
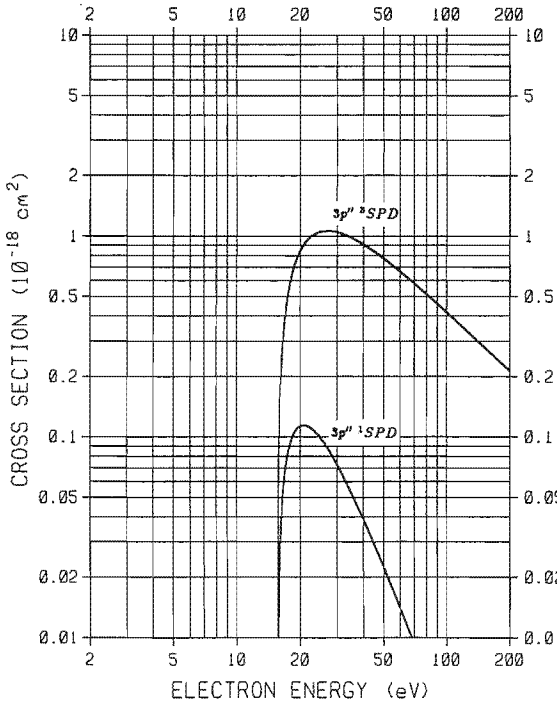
FIG. 17. O($^3P \to 3p''$ ^3SPD, $3p''$ ^1SPD) excitation cross sections.

Table 16. O($^3P \longrightarrow 3s''$ $^3P^o$, $3s''$ $^1P^o$) excitation cross sections.

Electron energy (eV)	σ (10^{-18} cm^2)	
	$3s''$ $^3P^o$	$3s''$ $^1P^o$
14.2	0.08	-
14.4	0.09	-
14.6	0.10	0.003
14.8	0.11	0.009
15	0.13	0.018
16	0.25	0.082
17	0.47	0.156
18	0.78	0.222
19	1.08	0.275
20	1.48	0.315
22	2.46	0.358
25	3.99	0.366
28	5.88	0.341
30	6.77	0.318
35	8.48	0.256
40	9.64	0.203
45	10.41	0.160
50	10.92	0.128
55	10.74	0.103
60	10.57	0.084
70	9.93	0.058
100	7.40	0.023
150	5.24	0.008
200	4.67	0.003
>200	$(-1170 + 397 \ln E)/E$	$2.4 \times 10^4 E^{-3}$

Table 17. O($^3P \longrightarrow 3p''$ ^3SPD, $3p''$ ^1SPD) excitation cross sections.

Electron energy (eV)	σ (10^{-18} cm^2)	
	$3p''$ ^3SPD	$3p''$ ^1SPD
15.8	0.092	0.016
16	0.155	0.028
17	0.416	0.070
18	0.608	0.095
19	0.747	0.108
20	0.849	0.113
21	0.923	0.114
22	0.976	0.112
23	1.012	0.108
25	1.051	0.099
28	1.058	0.083
30	1.044	0.073
35	0.982	0.053
40	0.909	0.039
45	0.838	0.029
50	0.773	0.022
55	0.716	0.018
60	0.665	0.014
70	0.581	0.009
100	0.418	0.003
150	0.282	0.001
200	0.213	0.0004
>200	$42.6E^{-1}$	$3.4 \times 10^3 E^{-3}$
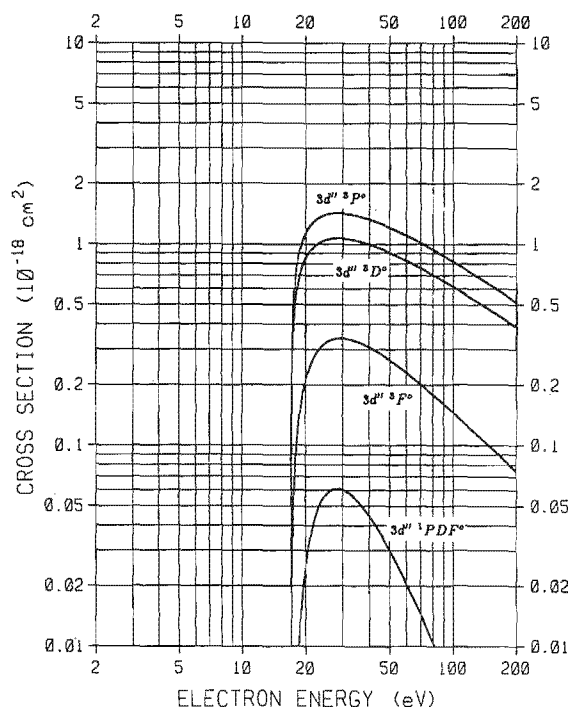
FIG. 18. $O(^3P \to 3d'' {}^3P^o, 3d'' {}^3D^o, 3d'' {}^3F^o, 3d'' {}^1PDF^o)$ excitation cross sections.

tion in the emission/autoionization branching ratio by 15% as allowed by the uncertainties of the branching ratio measurement (Dehmer *et al.*, 1977), coupled with a reasonabl estimate of the cascade contribution (e.g., 25% of the optica measurement), is still not enough to account for the discre pancies between the direct and optical cross sections.

The recent measurements, which are recommended have been fit to a curve by hand. The resulting profile for th transition is shown in Fig. 16; Table 16 gives the recom mended values. For $E > 200$ eV the cross sections are give by Eq. (3) with $F = 0.086$ (Doering *et al.*, 1985) an $A = -1.17 \times 10^{-15}$ cm^2 eV.

The $3s'' {}^1P^o$, $3p'' {}^3SPD$, and $3p'' {}^1SPD$ cross sections ar computed using Eq. (2) (with $\gamma = 0$) and the following: fo $3s'' {}^1P^o$, $W = 14.36$ eV, $\alpha = 1, \beta = 2, \Omega = 3$, and $F = 0.2$, $(3 - 1.19)^3 = 0.034$; for $3p'' {}^3SPD$, $W = 15.77$ eV, $\alpha = 2$ $\beta = 1, \Omega = 1$, and $F = 0.1/(3 - 0.86)^3 = 0.01$; and for $3p$ ^1SPD, $W = 15.99$ eV, $\alpha = 1, \beta = 1, \Omega = 3$, and $F = 0.04$, $(3 - 0.85)^3 = 0.004$ (Jackman *et al.*, 1977). The $3s'' {}^1P$ cross section is given in Fig. 16 and Table 16; the other tw cross sections are presented in Fig. 17 and Table 17.

2.5.b. $O(^3P \to 3d'' {}^3P^o, 3d'' {}^3D^o, 3d'' {}^3F^o, 3d'' {}^1PDF^o)$

No measurements of the $O(^3P \to 3d'' {}^3P^o, {}^3D^o)$ cros sections are available to our knowledge; therefore, we use th

Table 18. $O(^3P \longrightarrow 3d'' {}^3P^o, 3d'' {}^3D^o, 3d'' {}^3F^o, 3d'' {}^1PDF^o)$ excitation cross sections.

Electron energy (eV)	σ $(10^{-18}$ cm$^2)$			
	$3d'' {}^3P^o$	$3d'' {}^3D^o$	$3d'' {}^3F^o$	$3d'' {}^1PDF^o$
18	0.74	0.56	0.095	0.005
19	0.99	0.74	0.162	0.015
20	1.14	0.85	0.212	0.025
21	1.24	0.93	0.249	0.035
22	1.30	0.98	0.277	0.043
23	1.35	1.01	0.298	0.049
24	1.38	1.04	0.313	0.054
25	1.40	1.05	0.324	0.057
26	1.42	1.06	0.332	0.059
27	1.42	1.07	0.336	0.061
28	1.43	1.07	0.339	0.061
30	1.42	1.07	0.340	0.060
35	1.38	1.04	0.328	0.053
40	1.33	1.00	0.307	0.045
45	1.27	0.95	0.286	0.037
50	1.21	0.91	0.265	0.030
55	1.15	0.87	0.247	0.025
60	1.10	0.83	0.230	0.020
70	1.01	0.76	0.201	0.014
100	0.82	0.61	0.145	0.006
150	0.63	0.47	0.099	0.002
200	0.51	0.39	0.074	0.001
>200	$(-59 + 30.5 \ln E)/E$		$14.8E^{-1}$	
	$(-44 + 23 \ln E)/E$		$8 \times 10^3 E^{-3}$	

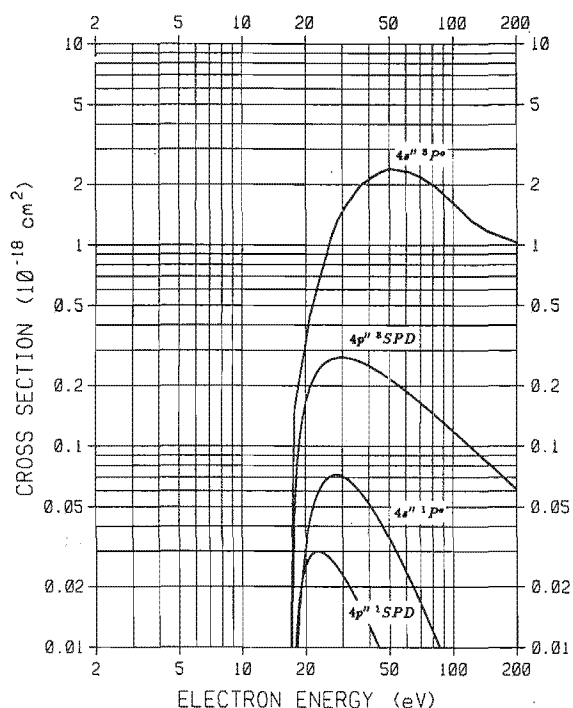FIG. 19. $O(^3P{\rightarrow}4s''\ ^3P^o, 4s''\ ^1P^o, 4p''\ ^3SPD, 4p''\ ^1SPD)$ excitation cross sections.

semi-empirical cross-section formula for optically allowed transitions of Jackman *et al.* (1977), given by

$$\sigma(E) = \frac{qF}{WE}\left[1 - \left(\frac{W}{E}\right)^\alpha\right]^\beta \ln\left(\frac{4EC}{W} + e\right), \qquad (15)$$

where σ, E, q, W, α, and β have been defined in Sec. 2.1.a.; e is the base of the natural logarithm; F is the optical oscillator strength; and C is an empirical parameter. For these excitations $W = 17.09$ eV, $\alpha = 1.26$, $\beta = 0.490$, and $C = 0.610$; for the $^3P^o$ state, $F = 0.008$, and for the $^3D^o$ state, $F = 0.006$ (Jackman *et al.*, 1977). The $^3P^o$ and $^3D^o$ cross sections are plotted as a function of electron-impact energy in Fig. 18; corresponding values are given in Table 18.

We might mention here that an attempt was made to fit by this formula the cross sections of the other allowed transitons for which good experimental data are available. For the $O(^3P{\rightarrow}3s''\ ^3P^o)$ cross section the fit is fairly good, using $F = 0.086$ (Doering *et al.*, 1985) and the other parameters from Jackman *et al.* (1977), but for all other cross sections considered, no good fit could be obtained.

The $3d''\ ^1F^o$ and $3d''\ ^1PDF^o$ cross sections are obtained using Eq. (2) (with $\gamma = 0$) and the following: for $3d''$ $^3F^o$, $W = 17.09$ eV, $\alpha = 2$, $\beta = 1$, $\Omega = 1$, and $F = 0.1/(3 - 0.05)^3 = 0.0039$; and for $3d''\ ^1PDF^o$, $W = 17.09$ eV,

Table 19. $O(^3P \longrightarrow 4s''\ ^3P^o, 4s''\ ^1P^o, 4p''\ ^3SPD, 4p''\ ^1SPD)$ excitation cross sections.

Electron energy (eV)	$\sigma\ (10^{-18}\ \text{cm}^2)$			
	$4s''\ ^3P^o$	$4s''\ ^1P^o$	$4p''\ ^3SPD$	$4p''\ ^1SPD$
17	0.02	-	-	-
18	0.17	0.008	0.065	0.012
19	0.24	0.020	0.122	0.020
20	0.33	0.032	0.164	0.026
21	0.45	0.043	0.196	0.028
22	0.54	0.052	0.220	0.030
23	0.65	0.059	0.238	0.030
24	·0.76	0.065	0.251	0.030
25	0.88	0.068	0.261	0.029
26	1.03	0.071	0.268	0.028
28	1.29	0.072	0.275	0.025
30	1.49	0.071	0.276	0.023
35	1.86	0.062	0.267	0.017
40	2.12	0.052	0.251	0.013
45	2.29	0.043	0.234	0.010
50	2.40	0.035	0.217	0.008
55	2.36	0.029	0.202	0.006
60	2.32	0.024	0.188	0.005
70	2.19	0.017	0.165	0.003
100	1.63	0.007	0.119	0.001
150	1.15	0.002	0.081	0.0003
200	1.03	0.001	0.061	0.00013
>200	$(-255 + 87\ \ln E)/E$	$12.2E^{-1}$		
		$8 \times 10^3 E^{-3}$		$1 \times 10^3 E^{-3}$

$\alpha = 1$, $\beta = 2$, $\Omega = 3$, and $F = 0.2/(3 - 0.05)^3 = 0.008$ (Jackman *et al.*, 1977). These cross sections are given in Fig. 18 and Table 18.

2.5.c. Transitons to $O^+(^2P^o)$-Core Rydberg States with $n=4$

The $O(^3P \rightarrow 4s''\,^3P^o)$ cross section is obtained by scaling the corresponding $n = 3$ profile using Eqs. (4) and (5), and data from Tables 1 and 2. The scale factor for the $n = 4$ cross section is 0.22. The resulting cross section is given in Fig. 19 and Table 19.

The $4s''\,^1P^o$, $4p''\,^3SPD$, and $4p''\,^1SPD$ cross sections are computed using Eq. (2) (with $\gamma = 0$) and the following: for $4s''\,^1P^o$, $W = 16.90$ eV, $\alpha = 1$, $\beta = 2$, $\Omega = 3$, and $F = 0.2/(4 - 1.19)^3 = 0.009$; for $4p''\,^3SPD$, $W = 17.24$ eV, $\alpha = 2$, $\beta = 1$, $\Omega = 1$, and $F = 0.1/(4 - 0.86)^3 = 0.003$; and for $4p''\,^1SPD$, $W = 17.25$ eV, $\alpha = 1$, $\beta = 1$, $\Omega = 3$, and $F = 0.04/(4 - 0.85)^3 = 0.0013$ (Jackman *et al.*, 1977). These cross sections are plotted in Fig. 19; values are tabulated in Table 19.

For the $O(^3P \rightarrow 4d''\,^3PD^o)$ cross section, we use the semi-empirical formula of Jackman *et al.* (1977), together with Eq. (5) for the F value. The result becomes

$$\sigma_4(E) = \frac{qF^*}{W_4 E (4 - \delta)^3} \left[1 - \left(\frac{W_4}{E} \right)^\alpha \right]^\beta \ln \left(\frac{4EC}{W_4} + e \right). \quad (16)$$

In Eq. (16): $F^* = 0.360$ (Jackman *et al.*, 1977); α, β, and C are the same as for the $n = 3$ cross section; W_4 is given in Table 1; and δ is given in Table 2. This cross section is plotted in Fig. 20 and tabulated in Table 20.

The $4d''\,^3F^o$ and $4d''\,^1PDF^o$ cross sections are obtained using Eq. (2) (with $\gamma = 0$) and the following: for $4d''\,^3F^o$, $W = 17.77$ eV, $\alpha = 2$, $\beta = 1$, $\Omega = 1$, and $F = 0.1/(4 - 0.05)^3 = 0.0016$; and for $4d''\,^1PDF^o$, $W = 17.77$ eV, $\alpha = 1$, $\beta = 2$, $\Omega = 3$, and $F = 0.2/(4 - 0.05)^3 = 0.0032$ (Jackman *et al.*, 1977). These cross sections are given in Fig. 20 and Table 20.

2.5.d. Transitions to $O^+(^2P^o)$-Core Rydberg States with $n \geqslant 5$

The $O(^3P \rightarrow \Sigma(n \geqslant 5) ns''\,^3P^o)$ cross section is obtained by scaling the $n = 3$ profile using Eq. (6), and data from Tables 1 and 2. The scale factor that results is 0.20 for this set of states. This cross section is presented in Fig. 21 and Table 21.

The $\Sigma(n \geqslant 5)\, ns''\,^1P^o$, $\Sigma(n \geqslant 5)\, np''\,^3SPD$, and $\Sigma(n \geqslant 5)\, np''\,^1SPD$ cross sections are computed using Eq. (2) (with $\gamma = 0$) and the following: for $ns''\,^1P^o$, $W = 18.16$ eV, $\alpha = 1$, $\beta = 2$, $\Omega = 3$, and $F = 0.2/[2(4.5 - 1.19)^2] = 0.009$; for $np''\,^3SPD$, $W = 18.22$ eV, $\alpha = 2$, $\beta = 1$, $\Omega = 1$, and $F = 0.1/[2(4.5 - 0.86)^2] = 0.0038$; and for $np''\,^1SPD$, $W = 18.22$ eV, $\alpha = 1$, $\beta = 1$, $\Omega = 3$, and $F = 0.04/[2(4.5 - 0.85)^2] = 0.0015$ (Jackman *et al.*, 1977). These cross sections are given in Fig. 21 and Table 21.

For the $O(^3P \rightarrow \Sigma(n \geqslant 5) nd''\,^3PD^o)$ cross section, we use the following semi-empirical formula of Jackman *et al.* (1977):
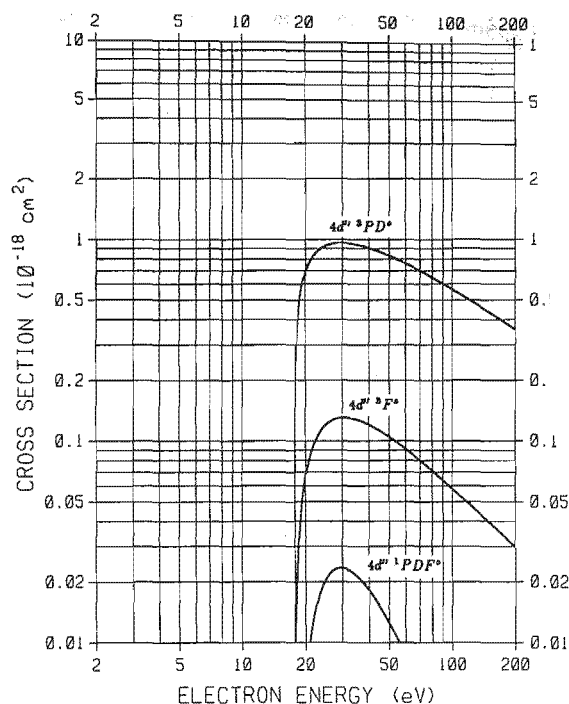
FIG. 20. $O(^3P \rightarrow 4d''\,^3PD^o, 4d''\,^3F^o, 4d''\,^1PDF^o)$ excitation cross sections.

TABLE 20. $O(^3P \rightarrow 4d''\,^3PD^0, 4d''\,^3F^0, 4d''\,^1PDF^0)$ excitation cross sections.

Electron energy (eV)	σ $(10^{-18}$ cm^2)		
	$4d''\,^3PD^o$	$4d''\,^3F^o$	$4d''\,^1PDF^o$
18	0.27	0.014	-
18.2	0.36	0.020	0.001
18.6	0.47	0.033	0.002
19	0.55	0.044	0.003
20	0.69	0.067	0.007
21	0.78	0.084	0.010
22	0.84	0.098	0.014
23	0.88	0.108	0.017
24	0.91	0.115	0.019
25	0.93	0.121	0.021
28	0.96	0.129	0.023
30	0.96	0.131	0.023
35	0.94	0.128	0.021
40	0.91	0.121	0.018
45	0.87	0.113	0.015
50	0.83	0.105	0.012
55	0.79	0.098	0.010
60	0.76	0.091	0.009
70	0.70	0.080	0.006
100	0.57	0.058	0.003
150	0.43	0.039	0.001
200	0.36	0.030	0.0004
>200	$(-44 + 22 \ln E)/E$	$6E^{-1}$	$3.4 \times 10^3 E^{-3}$

FIG. 21. $O(^3P \rightarrow \Sigma(n \geqslant 5)\ ns''\ ^3P^o$, $\Sigma(n \geqslant 5)\ ns''\ ^1P^o$, $\Sigma(n \geqslant 5)\ np''\ ^3SPD$, $\Sigma(n \geqslant 5)\ np''\ ^1SPD)$ excitation cross sections.

$$\sigma_{n>5}(E) = \frac{qF^*}{2W_A E(4.5-\delta)^2}$$

$$\times \left[1 - \left(\frac{W_A}{E}\right)^\alpha\right]^\beta \ln\left(\frac{4EC}{W_A} + e\right), \quad (17)$$

where F^*, α, β, and C are the same as given in the previous section, W_A is given in Table 1, and δ is given in Table 2. This cross section is shown in Fig. 22 and tabulated in Table 22.

The $\Sigma(n \geqslant 5)\ nd''\ ^3F^o$ and $\Sigma(n \geqslant 5)\ nd''\ ^1PDF^o$ cross sections are computed using Eq. (2) (with $\gamma = 0$) and the following: for $nd''\ ^3F^o$, $W = 18.35$ eV, $\alpha = 2, \beta = 1$, $\Omega = 1$, and $F = 0.1/[2(4.5-0.05)^2] = 0.0025$; and for nd'' $^1PDF^o$, $W = 18.35$ eV, $\alpha = 1$, $\beta = 2$, $\Omega = 3$, and $F = 0.2/[2(4.5-0.05)^2] = 0.005$ (Jackman et al., 1977). These cross sections are given in Fig. 22 and Table 22.

3. Electron-Impact Ionization Cross Sections

3.1. Single Ionization

For the single-ionization cross section of atomic oxygen, we use the measurements of Zipf (1985) and Brook et al. (1978). The data of Zipf, which cover the 40–300 eV
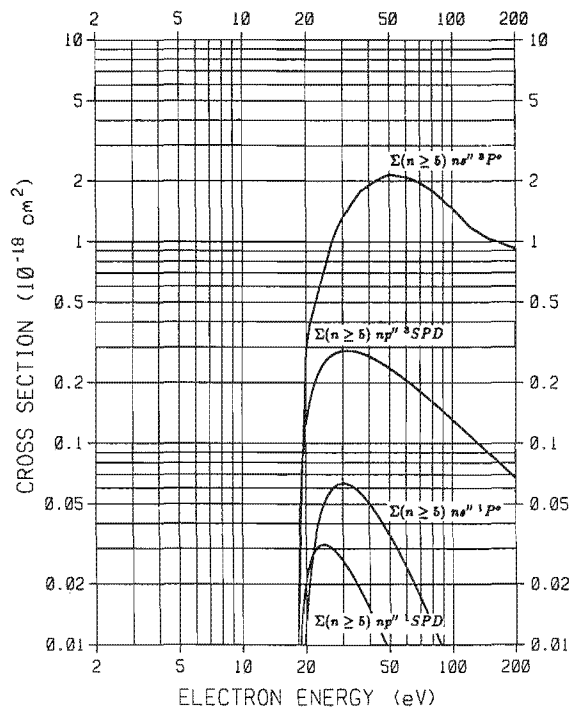
Table 21. $O(^3P \longrightarrow \Sigma(n \geq 5)\ ns''\ ^3P^o$, $\Sigma(n \geq 5)\ ns''\ ^1P^o$, $\Sigma(n \geq 5)\ np''\ ^3SPD$, $\Sigma(n \geq 5)\ np''\ ^1SPD)$ excitation cross sections.

Electron energy (eV)	σ $(10^{-18}$ cm$^2)$			
	$\Sigma(n \geq 5)\ ns''\ ^3P^o$	$\Sigma(n \geq 5)\ ns''\ ^1P^o$	$\Sigma(n \geq 5)\ np''\ ^3SPD$	$\Sigma(n \geq 5)\ np''\ ^1SPD$
18.6	0.02	0.002	0.04	0.007
18.8	0.03	0.003	0.05	0.010
19	0.05	0.004	0.07	0.012
20	0.29	0.013	0.12	0.021
21	0.40	0.023	0.17	0.026
22	0.48	0.033	0.20	0.029
23	0.58	0.041	0.22	0.031
24	0.68	0.048	0.24	0.031
25	0.79	0.053	0.26	0.031
28	1.16	0.062	0.28	0.028
30	1.34	0.063	0.29	0.026
35	1.67	0.059	0.28	0.020
40	1.90	0.051	0.27	0.015
45	2.05	0.042	0.25	0.012
50	2.15	0.035	0.24	0.009
55	2.12	0.029	0.22	0.007
60	2.08	0.024	0.21	0.006
70	1.96	0.017	0.18	0.004
100	1.46	0.007	0.13	0.001
150	1.03	0.002	0.09	0.0003
200	0.92	0.001	0.07	0.00013
>200	$(-229 + 78 \ln E)/E$	$8 \times 10^3 E^{-3}$	$13E^{-1}$	$1 \times 10^3 E^{-3}$

FIG. 22. O($^3P \rightarrow \Sigma(n \geqslant 5)$ nd'' $^3PD^o$, $\Sigma(n \geqslant 5)$ nd'' $^3F^o$, $\Sigma(n \geqslant 5)$ nd'' $^1PDF^o$) excitation cross sections.

impact energy range, are in very good agreement with the values of Brook *et al.*, which extend from threshold to 1000 eV. Moreover, according to Zipf, the absolute magnitudes of these data have an accuracy in the $\pm$ 5–10% range. The Brook *et al.* cross sections are recommended by Bell *et al.* (1983).

We allow branching to four different ion states: the usual outer-electron ionization states $^4S^o$, $^2D^o$, and $^2P^o$, and the inner ionization state $2s2p^4$ ^4P. For the ^4P state, we use the optical cross-section measurements of Zipf *et al.* (1985a; 1985b), which are in good agreement with the theoretical cross sections of Peach (1970). The branching ratios for direct ionization to the remaining three states of O$^+$ were calculated from theoretical ionization cross sections given by Peach (1968; 1971), and these were used to scale the experimental ionization cross section [after subtracting the ^4P and autoionization (see Sec. 4) contributions] to give the corresponding partial ionization cross sections. To these we must add the autoionization contribution, which we have assumed goes entirely into the O$^+$ ($^4S^o$) cross section, since most of the autoionizing states do not have large enough energies to excite the higher O$^+$ states.

The results are shown in Fig. 23 and tabulated in Table 23. Note that for impact energy $E > 1000$ eV we approximate the single-ionization cross section with the formula

Table 22. O($^3P \longrightarrow \Sigma(n \geq 5)$ nd'' $^3PD^o$, $\Sigma(n \geq 5)$ nd'' $^3F^o$, $\Sigma(n \geq 5)$ nd'' $^1PDF^o$) excitation cross sections.

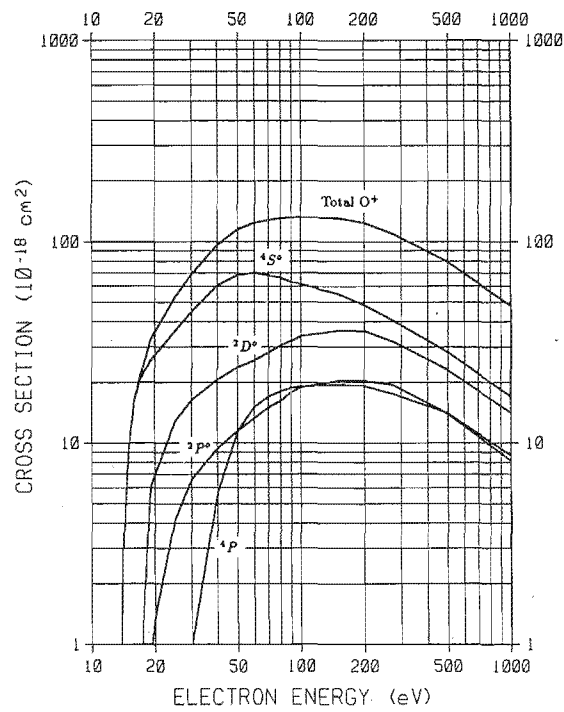| Electron energy (eV)	σ (10^{-18} cm^2)		
	$\Sigma(n \geq 5)$ nd'' $^3PD^o$	$\Sigma(n \geq 5)$ nd'' $^3F^o$	$\Sigma(n \geq 5)$ nd'' $^1PDF^o$
18.6	0.39	0.019	-
18.8	0.51	0.029	-
19	0.61	0.038	0.001
20	0.89	0.077	0.006
21	1.06	0.106	0.011
22	1.17	0.129	0.017
23	1.24	0.146	0.021
24	1.30	0.159	0.025
25	1.34	0.169	0.028
28	1.39	0.186	0.033
30	1.40	0.190	0.034
35	1.38	0.188	0.032
40	1.34	0.179	0.028
45	1.28	0.168	0.023
50	1.23	0.157	0.019
55	1.18	0.146	0.016
60	1.13	0.137	0.013
70	1.04	0.120	0.010
100	0.84	0.087	0.004
150	0.65	0.059	0.001
200	0.53	0.045	0.0004
>200	$(-63 + 32 \ln E)/E$	$9E^{-1}$	$3.4 \times 10^3 E^{-3}$

FIG. 23. $O(^3P) \to O^+(^4S^o, {}^2D^o, {}^2P^o, {}^4P)$ ionization cross sections.

$$\sigma(E) = \frac{A + B \ln E}{E} . \tag{18}$$

The parameters $A = -4.31 \times 10^{-14}$ cm^2 eV and $B = 1.32 \times 10^{-14}$ cm^2 eV give a reasonable high-energy fit. The branching ratios to the $^4S^o$, $^2D^o$, $^2P^o$, and ^4P states for $E > 1000$ eV are 0.36, 0.30, 0.17, and 0.18, respectively.

3.2. Double Ionization

The cross section for doubly ionizing atomic oxygen is only $\sim 1\%$ of the single-ionization cross section at 75 eV and about 4% at energies above 150 eV (Zipf, 1985). However, in some problems it still needs to be considered. We recommend use of the cross section measurements of Zipf (1985), which extend up to 300 eV. These measurements, with an accuracy of $\pm 5\%$–10%, are consistent with the data of Ziegler *et al.* (1982).
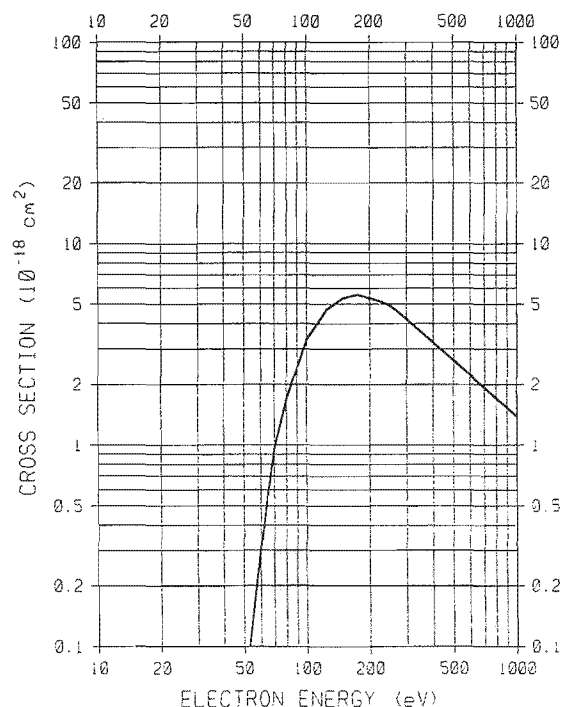
For $E > 300$ eV, the double-ionization cross section is approximated by Eq. (18) with $A = 6.60 \times 10^{-16}$ cm^2 eV and $B = 1.06 \times 10^{-16}$ cm^2 eV. The recommended values are shown in Fig. 24 and tabulated in Table 24.

4. Discussion

We have compiled a set of updated electron-bombardment cross sections for essentially all of the atomic oxygen

Table 23. $O(^3P) \longrightarrow O^+(^4S^o, {}^2D^o, {}^2P^o, {}^4P)$ ionization cross sections.

Electron energy (eV)	σ (10^{-18} cm^2)				
	$^4S^o$	$^2D^o$	$^2P^o$	^4P	Total
14	2.6	-	-	-	2.6
16	16.3	-	-	-	16.3
18	23.0	2.2	-	-	26.5
20	27.6	7.0	1.4	-	36.0
25	36.1	12.8	4.2	-	53.0
30	44.8	16.3	6.6	1.0	68.8
35	52.7	18.5	8.0	2.5	82.3
40	60.8	20.6	9.4	5.7	96.5
50	68.5	23.8	11.5	11.5	115.3
60	70.1	25.8	13.3	15.1	124.3
70	68.0	28.2	15.0	17.0	128.2
80	66.1	30.6	16.2	18.1	131.0
90	63.0	32.3	17.9	18.8	132.0
100	61.6	34.0	18.9	19.1	133.0
150	55.0	36.2	20.4	19.5	131.0
200	48.4	36.0	20.4	19.2	124.0
300	38.4	30.3	18.5	17.0	104.2
400	32.3	26.0	15.8	15.3	89.3
500	28.2	23.0	13.9	14.0	79.2
600	24.7	20.3	12.1	12.4	69.4
700	22.1	18.2	10.8	11.1	62.2
800	20.1	16.6	9.7	10.1	56.5
900	18.4	15.3	8.9	9.3	51.9
1000	17.1	14.2	8.2	8.7	48.1
	Fraction of total				
>1000	0.36	0.30	0.17	0.18	$(-43,100 + 13,200 \ln E)/E$

FIG. 24. $O(^3P) \to O^{2+}$ ionization cross section.

Table 24. $O(^3P) \longrightarrow O^{2+}$ ionization cross section. From Zipf (1985).

Electron energy (eV)	$\sigma \ (10^{-18} \ \text{cm}^2)$
60	0.296
65	0.563
70	0.963
80	1.68
90	2.42
100	3.34
125	4.72
150	5.38
175	5.59
200	5.37
225	5.17
250	4.93
275	4.57
300	4.22
400	3.24
500	2.64
600	2.23
700	1.94
800	1.71
900	1.54
1000	1.39
>1000	$(660 + 106 \ln E)/E$

excitation and ionization processes of practical interest.

In electron-impact calculations involving excitation and ionization, it is often important that autoionization be taken into account. The ionization cross sections given in Fig. 23 already include autoionization contributions and therefore these must be removed from the excitation cross sections in order to avoid overestimating the total inelastic cross section. The total excitation cross sections, both with and without autoionization contributions, and the ionization cross sections recommended in this report are plotted in Fig. 25 and tabulated in Table 25. The autoionizing excited-states of atomic oxygen and associated autoionization factors (i.e., branching ratios for ionization) are listed in Table 26. The autoionization factors given for the $2p^5 \ ^3P^o$, $3d''$ $^3P^o$, and $3s'' \ ^3P^o$ states were computed by taking a statistically weighted mean of the autoionization factors given for each $^3P_j^o$ fine-structure level by Dehmer et al. (1977). The errors for these data are at least $\pm 15\%$, and possibly larger. The autoionization factors for the remaining autoionizing states were obtained from Jackman et al. (1977); although the uncertainties associated with these numbers were not given, we surmise that they are larger than $\pm 15\%$.

In Fig. 25 the values used in the report by Slinker and Ali (1986) are also plotted for a quick overall comparison. The two sets of total ionization cross sections agree very well, since the recent measurements have differeed only slightly from the older measurements. The differences between the total excitation cross sections are greater, but still within a factor of 2. These differences between the total excitation cross sections are considerably smaller than the differences between many of the individual cross sections because some of the latter have been corrected upward and some
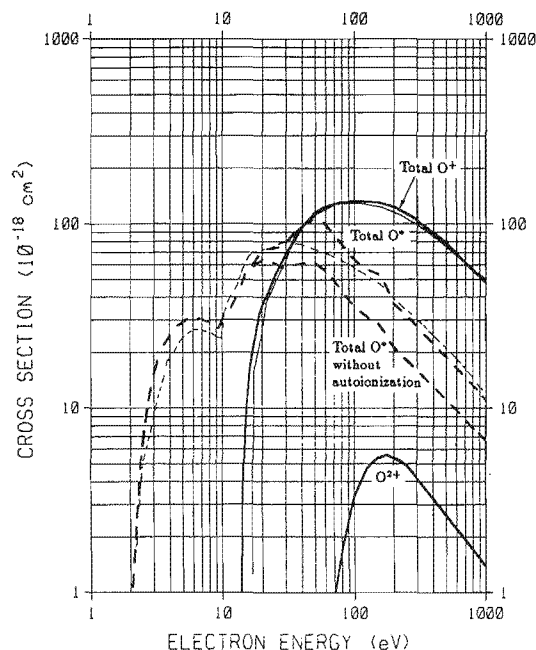

FIG. 25. Total $O(^3P) \to O^*$ excitation cross sections, with and without autoionization, and total $O(^3P) \to O^+$ and $O(^3P) \to O^{2+}$ ionization cross sections. The light solid and dashed lines are from Slinker and Ali (1986); the heavy solid and dashed lines are values recommended in this report.

Table 25. Total $O(^3P) \longrightarrow O^*$ excitation cross sections, with and without autoionization, and total inelastic cross sections.

Electron energy (eV)	σ (10^{-18} cm^2)		
	Excitation with autoionization	Excitation without autoionization	Inelastic
3	15.4	15.4	15.4
4	24.9	24.9	24.9
6	30.9	30.9	30.9
8	29.2	29.2	29.2
10	30.3	30.3	30.3
12	36.4	36.4	36.4
14	49.3	49.3	51.8
16	57.4	57.1	73.3
18	65.5	61.8	88.1
20	71.7	64.2	100
25	74.2	60.9	114
30	79.1	58.0	127
35	91.6	60.5	143
40	99.1	61.4	158
50	107.0	61.5	177
60	99.4	56.0	181
70	88.0	49.2	178
80	78.0	43.3	176
90	69.7	38.8	173
100	64.0	35.5	172
150	54.0	28.9	165
200	37.0	21.2	151
300	27.8	16.1	125
400	22.5	13.1	106
500	19.0	11.2	93.0
600	16.6	9.8	81.4
700	14.7	8.7	72.8
800	13.3	7.9	66.0
900	12.1	7.2	60.6
1000	11.1	6.6	56.1

Table 26. Autoionization factors for the autoionizing excited states.

State	A.F.
$O(2p^5\ ^3P^0)$	0.51
$O(3d'\ ^3S^0)$	0.50
$O(3d'\ ^3P^0)$	0.65
$O(3d'\ ^3D^0)$	0.50
$O(4s'\ ^3D^0)$	1.00
$O(4d'\ ^3SPD^0)$	0.70
$O(ns'\ ^3D^0)$	1.00
$O(nd'\ ^3SPD^0)$	1.00
$O(3s''\ ^3P^0)$	0.46
$O(3d''\ ^3P^0)$	0.30
$O(3d''\ ^3D^0)$	0.50
$O(4s''\ ^3P^0)$	1.00
$O(4d''\ ^3PD^0)$	0.75
$O(ns''\ ^3P^0)$	1.00
$O(nd''\ ^3PD^0)$	0.75

downward. However, in most applications it is not just the total excitation and ionization cross sections that matter, but also the branching ratios. The revised branching ratios presented in this report will have important effects on the relative production of different excited states and on the secondary electron distribution obtained in electron/oxygen scattering calculations.

5. Acknowledgments

6. References

Bell, K. L., H. B. Gilbody, J. G. Hughes, A. E. Kingston, and F. J. Smith, J. Phys. Chem. Ref. Data **12**, 891 (1983).

Brook, E., M. F. A. Harrison, and A. C. H. Smith, J. Phys. B **11**, 3115 (1978).

Dalgarno, A. and G. Lejeune, Planet. Space Sci. **19**, 1653 (1971).

Dehmer, P. M., W. L. Luken, and W. A. Chupka, J. Chem. Phys. **67**, 195 (1977).

Doering, J. P., E. E. Gulcicek, and S. O. Vaughan, J. Geophys. Res. **90**, 5279 (1985).

Erdman, P. W. and E. C. Zipf, J. Geophys. Res. **88**, 7245 (1983).

Erdman, P. W. and E. C. Zipf, Planet. Space Sci. **34**, 1155 (1986).

Gladstone, G. R., R. Link, S. Chakrabarti, and J. C. McConnel, J. Geophys. Res. **92**, 12445 (1987).

Gulcicek, E. E. and J. P. Doering, J. Geophys. Res. **92**, 3445 (1987).

Gulcicek, E. E. and J. P. Doering, J. Geophys. Res. **93**, 5879 (1988).

Gulcicek, E. E., J. P. Doering, and S. O. Vaughan, J. Geophys. Res. **93**, 5885 (1988).

Henry, R. J. W., P. G. Burke, and A.-L. Sinfailam, Phys. Rev. **178**, 218 (1969).

Jackman, C. H., R. H. Garvey, and A. E. S. Green, J. Geophys. Res. **82**, 5081 (1977).

Julienne, P. S. and J. Davis, J. Geophys. Res. **81**, 1397 (1976).

Meier, R. R., J. Geophys. Res. **87**, 6307 (1982).

Moore, C. E., NSRDS-NBS 3 (1976).

Morrison, M. D., Planet. Space Sci. **33**, 135 (1985).

Peach, G., J. Phys. B **1**, 1088 (1968).

Peach, G., J. Phys. B **3**, 328 (1970).

Peach, G., J. Phys. B **4**, 1670 (1971).

Rountree, S. P. and R. J. W. Henry, Phys Rev. A **6**, 2106 (1972).

Sawada, T. and P. S. Ganas, Phys. Rev. A **7**, 617 (1973).

Shyn, T. W. and W. E. Sharp, J. Geophys. Res. **91**, 1691 (1986).

Shyn, T. W., S. Y. Cho, and W. E. Sharp, J. Geophys. Res. **91**, 13751 (1986).

Slinker, S. and A. W. Ali, NRL Memorandum Report 5909 (1986).

Smith, E. R., Phys. Rev. A **13**, 65 (1976).

Stone, E. J. and E. C. Zipf, Phys. Rev. A **4**, 610 (1971).

Stone, E. J. and E. C. Zipf, J. Chem. Phys. **60**, 4237 (1974).

Thomas, L. D. and R. K. Nesbet, Phys. Rev. A **11**, 170 (1975).

Vaughan, S. O. and J. P. Doering, J. Geophys. Res. **91**, 13755 (1986).

Vaughan, S. O. and J. P. Doering, J. Geophys. Res. **92**, 7749 (1987).

Vaughan, S. O. and J. P. Doering, J. Geophys. Res. **93**, 289 (1988).

Vo Ky Lan, N. Feautrier, M. Le Dourneuf, and H. Van Regemorter, J. Phys. B **5**, 1506 (1972).

Ziegler, D. L., H. H. Newman, K. Smith, and R. F. Stebbings, Planet. Space Sci. **30**, 451 (1982).

Zipf, E. C., Planet. Space Sci. **33**, 1303 (1985).

Zipf, E. C. and P. W. Erdman, J. Geophys. Res. **90**, 11087 (1985).

Zipf. E. C., W. W. Kao, and R. W. McLaughlin, Chem. Phys. Lett. **118**, 591 (1985a).

Zipf. E. C., W. W. Kao, and P. W. Erdman, Planet. Space Sci. **33**, 1309 (1985b).

Zipf. E. C. and W. W. Kao, Chem. Phys. Lett. **125**, 394 (1986).